Copyright 2013 Rujing Zhang

RECONFIGURING THE SIDE-CHAIN FUNCTIONALITY OF CATIONIC HELICAL POLYPEPTIDES TOWARD MAXIMIZED GENE DELIVERY CAPABILITIES

BY

RUJING ZHANG

THESIS

Submitted in partial fulfillment of the requirements
for the degree of Master of Science in Materials Science and Engineering
in the Graduate College of the
University of Illinois at Urbana-Champaign, 2013

Urbana, Illinois

Adviser:

Professor Jianjun Cheng

ABSTRACT

The rational design of effective and safe non-viral gene vectors is largely dependent on the understanding of the structure-property relationship. This thesis aims to report the design of a new series of cationic, α-helical polypeptides with different side charged groups (amine and guanidine) and hydrophobicity, and to mechanistically unravel the effect of polypeptide structure on the gene delivery capability. Guanidine-containing polypeptides displayed superior membrane activities to their amine-containing analogues via the pore formation mechanism, and thus possessed notably higher transfection efficiencies. Elongating the hydrophobic side chain also potentiated the membrane activities of the polypeptides, while at the meantime caused higher cytotoxicities. Upon an optimal balance between membrane activity and cytotoxicity, maximal transfection efficiency was achieved which outperformed commercial reagent Lipofectamine™ 2000 (LPF2000) by 3-6 folds. This study thus provides mechanistic insights into the rational design of non-viral gene delivery vectors, and the top-performing materials identified also serve as promising additions to the existing systems.

ACKNOWLEDGEMENTS

The author wishes to express the sincere appreciation to Professor Jianjun Cheng for substantial mentoring and support to this project. In addition, special thanks to Dr. Lichen Yin for kind guidance in scientific research and assistance in the preparation of this manuscript. Thanks also to Nan Zheng and Ziyuan Song who continuously provided help and encouragement. Finally, thanks to my family and friends who have supported me unconditionally all along.

TABLE OF CONTENTS

Chapter 1: Introduction 1

Chapter 2: Experimental 5

Chapter 3: Results 15

Chapter 4: Discussion 22

Chapter 5: Conclusion 26

Figures and Tables 27

References 48

CHAPTER 1

INTRODUCTION

Thanks to advanced knowledge in molecular biology and genetic engineering, many disease-associated genes and their molecular regulators which provide potential targets for disease treatment have been successfully identified. Gene therapy, mediated by the transfer of genetic materials into target cells or tissues to promote or rectify the expression of specific genes, becomes a promising approach to treat human disease such as cancer, cystic fibrosis, arthritis, Gaucher disease and so on [1-3]. Due to the impermeability of genetic materials to cell membranes, the development of efficient yet biocompatible delivery vectors is crucial in the applications of gene therapy. Viral vectors have been long investigated and dominated current clinical trials [4, 5]. Despite their high efficiency, viral vectors present severe safety concerns such as carcinogenicity, immunogenicity and insertional mutagenesis [6]. Non-viral vectors, mostly cationic liposomes and polymers, possess desired biocompatibility and minimal mutagenesis and thus serve as alternatives to viral vectors for gene delivery [7-9].

Cell penetrating peptides (CPPs), exemplified by HIV-TAT, penetratin, transportan and Arg9, are sequence-specific oligopeptides that possess excellent membrane activities. It has been reported that CPPs often adopt inherent helical conformations or form helices during membrane transduction. Mechanistic simulation also suggests that the formation of a trans-membrane helix presents a rigid amphiphilic structure to stabilize the membrane interactions and promote the membrane permeability [10-15]. Due to their distinguished membrane permeability, CPPs are able to mediate the delivery of various cargos such as nucleic acids, proteins, peptides and even

nanoparticles. However, when utilized as gene delivery vectors, CPPs are often too short (fewer than 25 amino acid residues) and lack adequate cationic charge density. Hence, they are usually unable to function as stand-alone vectors to independently condense and subsequently deliver genes. Instead, they were incorporated or conjugated to existing delivery vectors as component material that could facilitate the cellular internalization and endosomal escape of the gene cargo [16-19]. Comparatively, polypeptides such as poly-L-lysine (PLL) and poly-L-arginine (PLR), were among the first set of materials adopted as non-viral vectors [20-22]. Although they are able to independently condense and deliver plasmid DNA due to the sufficient backbone length, they suffered from generally low transfection efficiency [23]. This is largely attributed to the fact that they adopt random coil conformation in the aqueous solution or when associated with phospholipid membranes because of the strong side chain charge repulsion, which hence severely comprised the membrane activities of these polypeptides with high molecular weight (MW) [13].

In order to address the disadvantages of both short CPPs and polypeptides towards gene delivery, we recently developed a strategy to stabilize the helical secondary conformation by positioning the side charged groups distally from the polypeptide backbone, such that the side-chain repulsion could be diminished and the helical structure could thus be stabilized [24]. A library of cationic polypeptides containing various amine side groups was thus synthesized and screened for their gene delivery capacities [25]. The top-performing material named PVBLG-8 was identified and thus exploited as an effective delivery vehicle of gene cargo, wherein its polymeric nature achieved the condensation of DNA and the stable helical structure contributed to its cell penetrating capability, notably outperforming traditional CPPs and polypeptides [26, 27]. Although such screening process allows the identification of desired materials, rational

design over polymer structure and mechanistic studies on the structure-function relationship would be more efficient and promising to further maximize gene transfection efficiency [28, 29].

Arginine (Arg) residues are often found rich in CPPs' primary structures, and the guanidine groups of the Arg residues have been closely tied to the functionalities of CPPs because of their interaction with the sulfate groups of glycosaminoglycans on cell membranes [30]. In addition, hydrophobicity also has significant effects on cell penetrating efficiency. Tew and *et al.* demonstrated that the incorporation of hydrophobic residues into CPPs or CPP mimics enhanced cell penetration property, termed a "self-activation" manner [31, 32]. Motivated by these understandings, we herein report the design of a new series of cationic, α-helical polypeptides with different side charged groups (amine and guanidine) and hydrophobicity, attempting to illuminate the effect of polymer structure and functionality on the gene transfection efficiency. We hypothesized that the incorporation of helical structures, guanidine groups and elongated hydrophobic side chains would endow the polypeptides with considerable advantages associated with gene delivery over conventional CPPs and polypeptides, and an optimal combination would thus lead to the maximization of the gene delivery capabilities of cationic helical polypeptides. Alkyne-functionalized *N*-carboxylanhydride (NCA) monomers were first polymerized via a controlled ring-opening polymerization method [33] and post-modified through "click" chemistry. Those two well-controlled and efficient chemistries rendered the resulting polypeptides with narrow molecular weight distributions (MWDs) and precise structures, presenting an ideal template for such studies on structure-function relationship. In two different mammalian cell lines (HeLa and COS-7), polypeptides with diverse structures were comprehensively studied in terms of their membrane activities, intracellular DNA delivery efficiencies, intracellular kinetics, transfection efficiencies and cytotoxicities. This fundamental

study hence provides insights into the rational design of non-viral gene delivery vectors and strategy to maximize gene transfection efficiency.

CHAPTER 2

EXPERIMENTAL

2.1. Materials and cell lines

All chemicals were purchased from Sigma-Aldrich (St. Louis, MO, USA) and used as received unless otherwise indicated. Anhydrous tetrahydrofuran (THF), hexane, and dimethylformamide (DMF) were dried by a column packed with 4Å molecular sieves and stored in a glovebox. Hexamethyldisilazane (HMDS) was dissolved in DMF in a glovebox and subsequently used to initiate the controlled ring-opening polymerization (ROP) of *N*-carboxyanhydride (NCA). Plasmid DNA encoding luciferase (pCMV-Luc) was purchased from Elim Biopharmaceutics (Hayward, CA, USA). YOYO-1, Lipofectamine^{TM} 2000 (LPF2000), and 3-(4,5-dimethylthiahiazol-2-yl)-2,5-diphenyl-2H-tetrazolium bromide (MTT) were purchased from Invitrogen (Carlsbad, CA, USA).

HeLa (human cervix adenocarcinoma) and COS-7 (African Green Monkey SV40-transf'd kidney fibroblast) were purchased from the American Type Culture Collection (Rockville, MD, USA) and were cultured in Dulbecco's Modified Eagle Medium (DMEM) (Gibco, Grand Island, NY, USA) containing 10% fetal bovine serum (FBS).

2.2. Instrumentation

^{1}H NMR spectra were recorded on a Varian U500 MHz or a VXR-500 MHz spectrometer. Gel permeation chromatography (GPC) experiments were conducted on a system equipped with an isocratic pump (Model 1100, Agilent Technology, Santa Clara, CA, USA), a DAWN

HELEOS multi-angle laser light scattering (MALLS) detector (Wyatt Technology, Santa Barbara, CA, USA), and an Optilab rEX refractive index detector (Wyatt Technology, Santa Barbara, CA, USA). The detection wavelength of HELEOS was set at 658 nm. Separations were performed using serially connected size exclusion columns (100 Å, 500 Å, 10^3Å and 10^4 Å Phenogel columns, 5 μm, 300 × 7.8 mm, Phenomenex, Torrance, CA, USA) at 60 ℃ using DMF containing 0.1 M LiBr as the mobile phase. The MALLS detector was calibrated using pure toluene and can be used for the determination of the absolute molecular weights (MWs). The MWs were determined based on the d*n*/d*c* value of each polymer sample calculated offline by using the internal calibration system processed by the ASTRA V software (version 5.1.7.3, Wyatt Technology, Santa Barbara, CA, USA). Circular dichroism (CD) experiments were performed on a JASCO J-815 CD spectrometer. Polypeptides were dissolved in deionized (DI) water at the concentrations of 0.025-0.2 mg/mL unless otherwise indicated. The solution was placed in a quartz cell with a light path of 1 or 10 mm. The mean residue molar ellipticity of each polypeptide was calculated based on the measured apparent ellipticity by following equations reported in literature: Ellipticity ([θ] in deg cm^2 dmol^{-1}) = (millidegrees × mean residue weight)/(pathlength in millimeters × concentration of polypeptide in mg mL^{-1}). The helicity of the polypeptides were calculated by the following formula: helicity = (-[θ_{222}] + 3000)/39000 [34]. In order to examine the helical stability of the polypeptides against pH, the pH of the polypeptide solution was accordingly adjusted with 1 M NaOH or 1 M HCl. The polypeptide concentration was fixed at 0.1 mg/mL for the pH and salt-dependent analyses.

2.3. Synthesis of the γ-(4-propargyloxybenzyl)-L-glutamic acid N-carboxyanhydride (POB-L-Glu-NCA) monomer

K_2CO_3 (15.2 g, 0.11 mol) and 4-hydroxybenzyl alcohol (9.3 g, 0.075 mol) were suspended in acetone (150 mL) into which propargyl bromide solution (80 wt% in toluene, 10 mL, 0.09 mol) and 18-crown-6 (0.1 mL) were added. The reaction mixture was refluxed at 75 ^oC for 12 h before removal of acetone by evaporation. Water (200 mL) was then added to the residue, and the aqueous layer was extracted with CH_2Cl_2 (DCM) (3 × 30 mL). The organic solutions were combined, washed with 15% NaOH solution (200 mL) and water (200 mL), and dried over Na_2SO_4. The product propargyloxybenzyl alcohol was obtained by removal of the solvent to yield clear yellow oil (9.7 g, yield 80%). ^1H NMR ($CDCl_3$): δ 7.28 (d, 2H, ArH), 6.94 (d, 2H, ArH), 4.67 (d, 2H, ArC*H*$_2$-), 4.60 (s, 2H, C*H*$_2$O-), 2.50 (t, 1H, *H*C≡C-).

The obtained propargyloxybenzyl alcohol (8.5 g, 52 mmol) was dissolved in DCM on an ice bath, and thionyl chloride (5 mL, 68 mmol) was added dropwise into the solution. The mixture was stirred at room temperature with the protection of nitrogen for 3.5 h, and water (100 mL) was then added to quench thionyl chloride. The organic layer was washed with water (3 × 50 mL) and dried over $MgSO_4$. The product propargyloxybenzyl chloride was obtained by removal of the solvent to yield clear yellow oil (7.0 g, yield 75%). ^1H NMR ($CDCl_3$): δ 7.31 (d, 2H, ArH), 6.94 (d, 2H, ArH), 4.68 (d, 2H, ArC*H*$_2$-), 4.55 (s, 2H, C*H*$_2$O-), 2.51 (t, 1H, *H*C≡C-).

$_L$-Glutamic acid copper (II) complex (3.29 g, 6.7 mmol) and $_L$-glutamic acid (1.99 g, 13.4 mmol) were suspended in a mixture of DMF (12 mL) and water (2 mL) into which 1,1,3,3-tetramethylguanidine (3.4 mL, 27 mmol) was added. The mixture was stirred at 40 ^oC for 2 h until all compounds were dissolved. DMF (10 mL) and the obtained propargyloxybenzyl chloride (6.5 g, 36 mmol) were added to the solution which was stirred at room temperature for 48 h. Acetone (200 mL) was then added, and the mixture was stirred overnight. The crude product was isolated and washed with acetone (4 times) and water (3 times), and

ethylenediaminetetraacetic acid disodium salt (EDTA-Na_2) solution (0.45 M) twice. The product γ-(4-propargyloxybenzyl)-$_L$-glutamic acid (POB-$_L$-Glu) was obtained via recrystallization from isopropanol/water (2:1, v/v) (3.2 g, yield 80%). ^{1}H NMR (DMSO-d_6/DCl-D_2O (20 wt %), 9:1, v/v): δ 7.30 (d, 2H, ArH), 6.96 (d, 2H, ArH), 5.00 (s, 2H, ArCH_2-), 4.77 (d, 2H, ArOCH_2-), 3.91 (m, 1H, α-H), 3.55 (t, 1H, *H*C≡C-), 2.54 (m, 2H, -C$H_2$$CH_2$COO-), 2.04 (m, 2H, -$CH_2CH_2$COO-).

POB-$_L$-Glu (1.15 g, 4.0 mmol) was dissolved in dry THF (25 mL) followed by addition of the phosgene solution (15 wt% in toluene, 4.0 mL, 5.6 mmol). The mixture was refluxed at 50 ℃ for 2 h. The solvent was removed under vacuum, and the crude product was recrystallized three times (THF/hexane, 1:5, v/v) to give γ-(4-propargyloxybenzyl)-$_L$-glutamic acid *N*-carboxyanhydride (POB-$_L$-Glu-NCA) as white crystals (770 mg, yield 61%). ^{1}H NMR ($CDCl_3$): δ 7.29 (d, 2H, ArH), 6.98 (d, 2H, ArH), 6.3 (s, 1H, N*H*), 5.08 (s, 2H, ArCH_2-), 4.70 (d, 2H, ArOCH_2-), 4.36 (t, 1H, α-H), 2.55 (m, 3H, -COC$H_2$$CH_2$-, *H*C ≡ C-), 2.04 (m, 2H, -CH_2CH_2COO-), 2.29-2.10 (m, 2H, -C$H_2$$CH_2$COO-).

2.4. Polypeptide synthesis

2.4.1. Polymerization of poly(γ-(4-propargyloxybenzyl)-$_L$-glutamate) (PPOBLG)

In a glovebox, POB-$_L$-Glu-NCA (100 mg, 0.32 mmol) was dissolved in DMF (1.5 mL), followed by the addition of the HMDS solution (64 μL, 0.1 mol/L, M/I = 50). The mixture was stirred at room temperature for 48 h (monomer conversion > 99% as monitored by FTIR), and most DMF was removed under vacuum. The final product PPOBLG was precipitated with cold methanol and collected as white solid. ^{1}H NMR ($CDCl_3$): δ 7.20 (d, 2H, ArH), 6.86 (d, 2H, ArH),

5.00-4.93 (d, 2H, ArCH_2-), 4.58 (s, 2H, ArOCH_2-), 3.98 (s, 1H, α-H), 2.62-2.49 (br, 3H, -CH_2CH_2COO-, HC≡C-), 2.29-2.12 (br, 2H, -CH_2CH_2COO-).

2.4.2. Synthesis of azido amines/guanidines

To obtain 3-azidopropylamine, sodium azide (5.85 g, 90 mmol) was added to a solution of 3-chloropropylamine hydrochloride (5.22 g, 45 mmol) in water (50 mL), and the mixture was heated at 80 ℃ for 24h. The pH was adjusted to 12 using 1 M NaOH, and the solution was extracted with diethyl ether (3 ×15 mL). The organic layer was dried over Na_2SO_4 and the solvent was removed under vacuum to obtain colorless oil (1.0 g, yield 30%). ^{1}H NMR ($CDCl_3$): δ 3.28 (t, 2H, -CH_2N_3), 2.71 (t, 2H, -CH_2NH_2), 1.61 (m, 2H, -$CH_2CH_2N_3$).

To obtain *N*,*N*-dimethyl-3-azidopropylamine, sodium azide (1.3 g, 20 mmol) was added to an aqueous solution of 3-dimethylamino-1-propyl chloride (1.58 g, 10 mmol, 20 mL), and the mixture was stirred at 70 ℃ for 12 h. KOH (5.0 g) was then added, and the aqueous solution was extracted with ether (3 × 15 mL). The combined organic phases was dried over Na_2SO_4 and concentrated to give colorless oil (0.98 g, yield 77%). ^{1}H NMR ($CDCl_3$): δ 3.34 (t, 2H, -CH_2N_3), 2.35 (t, 2H, -C$H_2N(CH_3)_2$), 2.25 (s, 6H, -N(CH_3)$_2$), 1.75 (m, 2H, -$CH_2CH_2N_3$).

To obtain 3-azidopropylguanidine, azidopropylamine (1.0 g, 10 mmol), H-pyrazole-1-carboxamidine hydrochloride (1.47 g, 10 mmol), and DIEA (1.74 mL, 10 mmol) were dissolved in dry DMF (15 mL) which was stirred at room temperature overnight. Ether (150 mL) was added to precipitate the crude product which was collected, washed with ether, and dried under vacuum to obtain yellow liquid (1.0 g, yield 60%). ^{1}H NMR ($CDCl_3$): δ 3.33 (t, 2H, -CH_2NHC(NH)NH_2), 3.18 (t, 2H, -CH_2N_3), 1.76 (m, 2H, -$CH_2CH_2N_3$).

The synthesis of 6-azidohexylguanidine was carried out using the same method with 6-azidohexylamine as the starting material. ^{1}H NMR ($CDCl_3$): δ 3.35 (t, 2H, -C*H*$_2$NHC(NH)NH$_2$), 3.20 (t, 2H, -C*H*$_2$N$_3$), 1.77 (m, 2H, -C*H*$_2$CH$_2$NHC(NH)NH$_2$), 1.67 (m, 2H, -C*H*$_2$CH$_2$N$_3$), 1.32 (m, 4H, -(C*H*$_2$)$_2$(CH$_2$)$_2$N$_3$).

The synthesis of 8-azidooctylguanidine was carried out using the same method with 8-azidooctylamine as the starting material. ^{1}H NMR ($CDCl_3$): δ 3.35 (t, 2H, -C*H*$_2$NHC(NH)NH$_2$), 3.20 (t, 2H, -C*H*$_2$N$_3$), 1.79 (m, 2H, -C*H*$_2$CH$_2$NHC(NH)NH$_2$), 1.70 (m, 2H, -C*H*$_2$CH$_2$N$_3$), 1.53-1.02 (m, 8H, -(C*H*$_2$)$_4$(CH$_2$)$_2$N$_3$).

2.4.3. Synthesis of amine/guanidine functionalized polypeptides

In a glovebox, PPOBLG (20 mg, 0.072 mmol alkyne groups) was dissolved in DMF (1.0 mL) into which various azido amines/guanidines (0.144 mmol) and *N*,*N*,*N*′,*N*″,*N*″-pentamethyldiethylenetriamine (PMDETA, 30 μL, 0.144 mmol) were added. CuBr (20.8 mg, 0.144 mmol) was then added, and the reaction mixture was stirred at room temperature for 24 h before addition of 1M HCl (1 mL). The final polypeptides were purified by dialysis against water for 3 days (MWCO = 3 kDa) and obtained after lyophilization. The nomenclature of polypeptides was summarized in **Table 1**.

2.5. Polyplex formation and characterization

Polypeptide and pCMV-Luc were separately dissolved in water at 0.2 mg/mL and mixed at various nitrogen/phosphate (N/P) ratios. The mixture was vortexed for 5 s and incubated at 37 ℃ for 30 min to allow polyplex formation. The resultant polyplexes were subject to electrophoresis in 1% agarose gel at 100 V for 45 min to qualitatively evaluate DNA

condensation by the polypeptides. To quantitatively monitor the DNA condensation level, the ethidium bromide (EB) exclusion assay [35] was conducted. Basically, EB solution was mixed with DNA at the DNA/EB ratio of 10:1 (w/w) and incubated at room temperature for 1 h. Polypeptide was then added to the mixture at various N/P ratios, and the mixture was further incubated at room temperature for 30 min before quantification of the fluorescence intensity on a microplate reader (λ_{ex} = 510 nm, λ_{em} = 590 nm). A pure EB exclusion and the DNA/EB solution without any polypeptide were used as negative and positive controls, respectively. The EB exclusion efficiency (% DNA condensed) was defined as the following:

$$\text{EB exclusion efficiency } (\%) = (1 - \frac{F - F_{EB}}{F_0 - F_{EB}}) \times 100$$

Where F_{EB}, F, and F_0 denote the fluorescence intensity of pure EB solution, DNA/EB solution with polypeptide, and DNA/EB solution without any polypeptide, respectively.

Particle size and zeta potential of polyplexes freshly prepared either in DI water or phosphate buffered saline (PBS) were further evaluated by dynamic laser scattering (DLS) on a Malvern Zetasizer (Herrenberg, Germany). To evaluate their stability against dilution, polyplexes were diluted with PBS for 50 folds, incubated at room temperature for different time, and subjected to particle size measurement.

2.6. In vitro gene transfection

Cells were seeded on 96-well plates at 1×10^4 cells/well and cultured in serum-containing DMEM medium for 24 h. The medium was then replaced by opti-MEM (100 μL/well), into which polyplexes were added at 0.1 μg DNA/well. After incubation at 37 ^{o}C for 4 h, the medium was replaced by serum-containing DMEM and cells were further incubated for another 20 h. Luciferase expression was assayed in terms of luminescence intensity using a Bright-Glo

luciferase assay kit (Promega, Madison, WI, USA), and the cellular protein level was determined using a BCA kit (Pierce, Rockford, IL, USA). Results were expressed as relative luminescence unit (RLU) associated with 1 mg of cellular protein (RLU/mg protein). In order to evaluate the transfection efficiency of polyplexes in the presence of serum, cells were incubated with polyplexes in DMEM supplemented with 10% FBS for 4 h. To further probe the temperature-dependent transfection capabilities, cells were incubated with polyplexes in opti-MEM at 4 ^{o}C for a 4-h uptake period before further incubation at 37 ^{o}C for 20 h. LPF2000 was used as a control according to the manufacture's protocol in all above-mentioned studies.

2.7. Membrane activity

The membrane activity of the polypeptides was evaluated by measuring the cellular uptake level of a membrane-impermeable dye, fluorescein isothiocyanate (FITC) in its non-reactive form (fluorescein-tris(hydroxymethyl)methanethiourea, FITC-Tris) [36]. Cells were seeded on 96-well plates at 1×10^4 cells/well and cultured for 24 h. The medium was replaced by opti-MEM (100 μL/well), into which FITC-Tris and the polypeptide were added at 1 μg/well and 2 μg/well, respectively. After incubation at 37 ℃ for 2 h, cells were washed with PBS containing heparin (20 U/mL) for three times and then lysed with the RIPA lysis buffer (100 μL/well). The amount of FITC-Tris in the cell lysate was quantified by spectrofluorimetry (λ_{ex} = 488 nm, λ_{em} = 530 nm), and the protein content was determined by the BCA kit. The uptake level was represented as ng FITC associated with 1 mg of cellular protein (ng FITC/mg protein). Cells incubated with free FITC-Tris in the absence of polypeptides were included as a negative control. Commercial CPPs, such as HIV-TAT, Arg9, and poly-$_L$-arginine (PLR) were used as internal controls.

2.8. Intracellular kinetics

DNA (1 mg/mL) was labeled with YOYO-1 (20 μM) at one dye molecule per 50 bp DNA in order to allow the quantification of the cellular uptake level [37]. YOYO-1-DNA was then allowed to form polyplexes with polypeptides at various N/P ratios as described above. Cells were seeded on 96-well plates at 1×10^4 cells/well and cultured for 24 h. The medium was replaced by opti-MEM followed by addition of the polyplexes at 0.1 μg YOYO-1-DNA/well. After incubation at 37 ℃ for 4 h, cells were washed with PBS containing heparin (20 U/mL) for four times to remove membrane-bound polyplexes, and were subsequently lysed with the RIPA lysis buffer (100 μL/well). YOYO-1-DNA content in the lysate was quantified by spectrofluorimetry (λ_{ex} = 485 nm, λ_{em} = 530 nm), and the protein content was determined using the BCA kit. Cellular uptake level was expressed as ng YOYO-1-DNA associated with 1 mg of cellular protein (ng YOYO-1-DNA/mg protein).

To probe the internalization mechanism of the polyplexes, the cellular uptake study was also performed at 4 ℃ or in the presence of various endocytic inhibitors. Briefly, cells were incubated with polyplexes (N/P = 10) at 4 ℃ for 2 h wherein the energy-dependent endocytosis was blocked. Otherwise, cells were incubated with various endocytic inhibitors including chlorpromazine (10 μg/mL), methyl-β-cyclodextrin (mβCD, 5 mM) and wortmannin (10 μg/mL) for 30 min prior to the addition of the polyplexes and throughout the 2-h uptake study. Results were represented as percentage uptake level of control cells that were incubated with the polyplexes in the absence of inhibitors at 37 ℃ for 2 h.

The cellular internalization and distribution of polyplexes were further visualized by confocal laser scanning microscopy (CLSM, LSM 700, Zeiss, Germany). HeLa cells were

seeded on the coverslip in 6-well plate at 1×10^5 cells/well and cultured for 24 h. The medium was replaced with opti-MEM (1.5 mL/well), and polypeptide/YOYO-1-DNA polyplexes (N/P = 10) were added at 1 μg YOYO-1-DNA/well before incubation at 37 ℃ for 4 h. Cells were then washed with heparin-PBS for four times, fixed with 4% paraformaldehyde (PFA), stained with DAPI (2 μg/mL) and Lysotracker®-Red (200 nM) before CLSM observation.

2.9. Cytotoxicity

Cells were seeded on 96-well plates at 1×10^4 cells/well and cultured for 24 h. The medium was replaced by opti-MEM (100 μL/well) into which polyplexes (N/P = 10) were added at 0.1, 0.2, 0.4, 1 and 2 μg DNA/well. After incubation at 37 ^{o}C for 4 h, the medium was replaced by serum-containing DMEM and cells were further incubated for another 20 h in consistence with the transfection process. Cell viability was then evaluated by the MTT assay. Cells without polyplex treatment served as the control and results were represented as percentage viability of control cells.

2.10. Statistical analysis

Statistical analysis was performed using Student's *t*-test and differences between test and control groups were judged to be significant at $*p < 0.05$ and very significant at $**p < 0.01$.

CHAPTER 3

RESULTS

3.1. Synthesis and characterization of the polypeptides.

PPOBLG was polymerized via ROP of POB-L-Glu-NCA mediated by HMDS, followed by the side-chain modifications through the azide-alkyne Huisgen cycloaddition, the well-known "click" chemistry [38]. HMDS-mediated polymerization allowed a controlled ROP, yielding well-defined polypeptide with narrow MWDs (~1.05) and desired degree of polymerization (DP = 49 at the monomer/initiator ratio of 50) as evidenced by the GPC traces (**Figure 4**). Due to the high efficiency of the "click" chemistry, the conjugation efficiency of amine- or guanidine-containing side chains reached over 90% based on ^{1}H NMR spectra (**Figure 7-13**). All the polypeptides were soluble in aqueous solutions at pH < 9, and adopted typical α-helical conformations as determined by the characteristic double-minima ellipticity at 208 and 222 nm in the CD spectra, distinctively different from the spectrum of poly(arginine) that adopts random coil conformation (**Figure 14A, 15**). The calculated helicity was similar among the guandinine-containing polypleptides (52~59%) and slightly higher for the amine-containing polypeptides (60% and 71%). Indicated by the ellipticities at 222 nm, the helicities of all test polypeptides were proven to remain stable within the concentration range of 0.025-0.2 mg/mL, suggesting that they were well dispersed in aqueous solutions despite the hydrophobic contents on the side chains (**Figure 14B**) [24]. The helicities maintained stable within the pH range of 1-9 (**Figure 14C**), enabling the polypeptides to exert their conformation-dependent membrane activities within a pH gradient from the neutral extracellular pH to the acidic endocytic compartments pH

(endosomes and lysosomes). As such, polypeptides with such helical stability would be capable of facilitating intracellular internalization as well as endosomal escape of the gene cargo by destabilizing/disrupting the cellular/endosomal membranes [26]. The helicities were also stable against ionic strength up to 0.3 M (**Figure 14D**), indicating that the helical conformations would be well maintained for all test polypeptides under physiological conditions with the ionic strength of approximately 0.15 M.

3.2. Polyplex formation and characterization

DNA condensation by the polypeptides was characterized by the gel retardation assay (**Figure 16A**). All the polypeptides were able to effectively condense DNA even at the N/P ratio of 2, indicated by the restricted DNA migration in the gel electrophoresis. In consistence, a quantitative EB exclusion assay further demonstrated that more than 70% of the DNA was condensed by the polypeptides at N/P rations higher than 5 (**Figure 16B**). Guanidine-containing polypeptides displayed slightly higher affinity for DNA than their amine-containing analogues, presumably because guanidine residues could form bidentate hydrogen bonding with phosphates on DNA molecules to render additional binding affinities [39]. The particle size and zeta potential of the formed polyplexes were further characterized by DLS. As shown in **Figure 17**, all the polypeptides were able to form 100~200 nm nanocomplexes with DNA in water at the N/P ratio higher than 5 with positive charges on surfaces. The polyplexes formed by guanidine-containing polypeptides displayed higher zeta potentials (~40 mV) than those formed by amine-containing polypeptides (~25 mV), probably because of the higher pKa value of guanidine groups. Polyplexes were also prepared and characterized in buffer solution (0.2 M PBS) to test their stability under physiological conditions. Higher N/P ratio up to 20 was required to form

stable polyplexes with comparable particle size (except T3), which was largely attributed to the charge screening effect induced by the excessive ions in the buffer solution that decrease the electrostatic attractions between the positively charged polypeptides and negatively charged DNA (**Figure 17C**). When polyplexes prepared in PBS were further diluted with PBS for 50 folds, the particle size remained relatively unaltered within 1.5 h, suggesting the desired stability of polyplexes against ionic strength and dilution (**Figure 17D**).

3.3. In vitro gene transfection

The transfection efficiencies of polypeptides containing different side charged groups yet the fixed side chain length (P3, T3, G3) were first evaluated in HeLa and COS-7 cells in serum-free medium. As shown in **Figure 18**, the polypeptide bearing guanidine groups exhibited significantly higher transfection efficiency than its amine-containing counterparts, suggesting that the guanidine groups were crucial in terms of mediating effective gene transfection presumably due to their membrane activities. G3 showed notably higher transfection efficiency by nearly two orders of magnitude than PLR adopting random coil conformation, which further highlighted the importance of helicity. The hydrophobic moieties can "self-activate" the membrane activities of guanidine groups, and thus we compared the transfection efficiencies of polypeptides bearing guanidine side charged groups yet different side chain length (G3, G6, G8). As shown in **Figure 19A and 19B**, in both cell lines, polypeptides with longer hydrophobic side chains exhibited higher transfection efficiencies at low N/P ratios (2.5 and 5), which confirmed the design strategy to enhance the gene delivery capacities of cationic helical polypeptides by introducing extra hydrophobic contents. When the N/P ratio was further elevated to 10 and 15, G6 demonstrated maximal transfection efficiency among those three polypeptides in HeLa cells

while G6 and G8 showed comparably high transfection efficiencies in COS-7 cells. The transfection efficiency decreased rather than kept increasing when the N/P ratio was increased up to 20, mainly due to the material-induced cytotoxicity at higher dosages. Polypeptides bearing primary amine groups yet different side chain length were also synthesized and tested in gene transfections. However, they all suffered from relatively low efficiencies although the increment in the transfection efficiency with the elongated side chains was also observed (**Figure 20**). With the collective effect of both guanidine and hydrophobic domains, G6 and G8 outperformed the commercial transfection reagent, LPF2000, by 2.5~5.5 folds in terms of the *in vitro* transfection efficiency (**Figure 19A, 19B**).

Since serum has been reported to inhibit the efficiencies of polycation based non-viral gene delivery vectors [40], transfections were thus performed in the presence of serum (10%FBS) as well. At the same DNA amount (0.1 μg/well) and N/P ratio, greatly compromised gene transfection efficiency was noted for all test polypeptides (**Figure 19C, 19D**), presumably because the anionic proteins in the serum would destabilize the polyplexes. However, the transfection efficiency can be largely recovered when the total amount of DNA or the N/P ratio was increased, indicating that excessive amount of polypeptides might counteract serum binding. G8 showed higher resistance against serum than G3 and G6 at lower DNA amount (0.1 μg/well), probably because the extra hydrophobicity mediated stronger interactions between the polypeptides and DNA, thus partially compensating the competitive replacement by serum. When the DNA amount was increased to 0.2 μg/well, G6 reached maximal transfection efficiencies in HeLa cells while G6 and G8 were equally competent in COS-7 cells, similar to the transfection capacities in the absence of serum.

3.4. Intracellular kinetics

The performance of non-viral gene delivery vectors is closely connected to their intracellular kinetics, such as the cellular uptake level, internalization pathway and endosomal escape mechanism [41]. We therefore probed the intracellular kinetics of the polypeptide/DNA polyplexes in attempts to provide mechanistic understandings on their gene delivery capacities.

As shown in **Figure 21**, all test polypeptides were able to remarkably promote the cellular uptake of YOYO-1-DNA, outperforming LPF2000 by 4-8 folds. Polypeptides bearing guanidine and primary amine side charged groups (G3 and P3) displayed comparable cellular uptake level which was higher than that of the tertiary amine-containing polypeptide (T3). Notable increase in the cellular uptake level was also observed when the hydrophobic side chain was elongated (G3, G6, G8), which suggested that hydrophobic content activated the guanidine groups to provide the polypeptides with higher membrane activities.

The internalization pathway determines the intracellular fate and ultimately affects the gene transfection capabilities of non-viral gene delivery vectors, and guanidine-rich CPPs have also been reported to promote the cellular internalization through a non-endocytic, direct translocation pathway [30, 42]. As such, cellular uptake studies were performed under various conditions that are known to inhibit specific uptake pathway in order to elucidate the internalization mechanism. Energy-dependent endocytosis was completely blocked at low temperature (4 ^{o}C) [43]. Chlorpromazine inhibited clathrin-mediated endocytosis (CME) by inducing the dissociation of the clathrin lattice; mβCD inhibited caveolae by depleting cholesterol; wortmannin inhibited macropinocytosis by inhibiting phosphatidyl inositol-3-phosphate [41]. As shown in **Figure 22A**, the cellular uptake level at 4 ^{o}C was only inhibited by 30% compared to that at 37 ^{o}C, suggesting that majority of the formed polyplexes entered cells

via an energy-independent and non-endocytosis pathway. In terms of those energy-dependent processes, mβCD induced the strongest inhibition on the cellular uptake level (~40%) while chlorpromazine and wortmannin only exhibited slight inhibitory effects, indicating that the polyplexes were internalized mainly through caveolae rather than CME and macropinocytosis. Compared to CME, caveolae is a non-acidic and non-digestive route of internalization, and therefore cargos in the caveosomes can be directly transported to the Golgi and/or endoplasmic reticulum [41]. Thereby, they would not undergo endosomal entrapment and lysosomal degradation, which largely contributed to the relatively high gene transfection efficiencies of the guanidine-containing helical polypeptides. Such statement was also supported by CLSM imaging, which was utilized to visualize the intracellular distributions of polyplexes, with polypeptide G6 in HeLa cells as example. The internalized polyplexes (green fluorescence) were largely separated from the Lysotracker-stained endosomes/lysosomes (red fluorescence, **Figure 22E**), indicating that they did not experience severe endosomal entrapment which posed as one of the major intracellular barriers against efficient gene delivery [44]. In consistence with the internalization mechanism, transfection efficiency at 4 ^{o}C was still relatively high, despite the notable decrease compared to that at 37 ^{o}C (**Figure 22B**).

Because a large amount of the polyplexes was internalized via direct translocation rather than endocytosis, the ability of the polypeptides to cause pore formation on cell membranes was then investigated, an important membrane penetration mechanism induced by the helical polypeptide [26, 37, 45, 46]. FITC-Tris, a membrane-impermeable fluorescent dye in the non-reactive form of FITC after reaction of FITC with Tris [36], was used as a biomarker, and the pore formation level on cell membranes was monitored by the cellular uptake level of FITC-Tris after co-incubation with the polypeptides. Free FITC-Tris was minimally internalized by cells,

however, treatment with the polypeptides led to substantial increase in cellular uptake of FITC-Tris (**Figure 22C, 22D**), substantiating that the guanidine-containing helical polypeptides were able to destabilize cell membranes by pore formation mechanism and subsequently allow the direct diffusion of FITC-Tris into the cytoplasm. Such pore formation capacities were further enhanced with the increment of hydrophobic contents. In comparison, the random-coiled PLR and other short CPPs including HIV-TAT and Arg9, demonstrated significantly lower pore formation properties. Such pore formation mechanism of polypeptides thus allowed direct permeation of the gene cargos into cells, and accordingly internalized YOYO-1-DNA was distributed to the whole cytoplasm in a permeated manner without being entrapped in endosomal/lysosomal compartments as shown in CLSM images (**Figure 22E**).

3.5. Cytotoxicity

Cytotoxicity of the polypeptide/DNA polyplexes (N/P = 10) at different DNA concentrations were assessed in both HeLa and COS-7 cells by the MTT assay. As shown in **Figure 23**, the cytotoxicity was both dose- and cell line-dependent. Guanidine-containing polypeptides displayed higher cytotoxicity than the amine-containing ones, and the polypeptides with longer side chains showed higher cytotoxicity in both cell lines, which correlated well with their pore formation capabilities. For each individual polypeptide, its toxicity towards HeLa cells was higher than towards COS-7 cells, presumably due to the different tolerability of each cell line towards material-induced cytotoxicity.

CHAPTER 4

DISCUSSION

Non-viral gene delivery vectors have emerged as promising alternatives to viral vectors due to their accessibility and safety profile. However, the major drawback of non-viral gene delivery is low transfection efficiency, stemming from multiple extra- and intracellular barriers associated with delivery process [44]. Above all, vectors should be able to effectively condense DNA into nano-scale complexes, maintain relatively stable under physiological conditions and then mediate efficient cellular uptake either via endocytosis or non-endocytic pathway. Among the existing polymer-based materials adopted as non-viral vectors, most of them possess cationic amine groups that could be protonated under physiological conditions and then could condense DNA to form polyplexes, such as poly(ethylenimine) (PEI), PLL and poly(amidoamine) dendrimer (PAMAM). Further modifications/conjugations, exemplified by modification with targeting moieties and PEGylation, could further promote the delivery efficiency and reduce the material cytotoxicity induced by excessive cationic charges [47]. Studies have also shown that such polyplexes are often internalized via endocytosis [48, 49], which leads to the transport of polyplexes from early endosomes to lysosomes filled with hydrolytic enzymes. Therefore, endosomal entrapment poses one major barrier that impedes the efficacy of non-viral vectors. PEI, one of the most widely used non-viral vectors containing large amount of primary, secondary and tertiary amine groups, is able to buffer the acidic environment in lysosomes, cause extra protons being pumped into the compartments, and finally osmotically rupture the lysosomes by the influx of counter ions, commonly known as the “proton sponge” effect [50].

However, this hypothesis has been debated and recent studies have suggested that the incorporation of amine groups with buffering capacity does not necessarily result in effective endosomal escape [51, 52]. At later stage, DNA needs to be released from complexes and transported from cytoplasm to the nuclei in order to initiate successful transcription.

Compared with amine groups, guanidine groups could bind DNA phosphate anions to form characteristic pairs of parallel hydrogen bonds, which stabilize the binding by not only their charge but also their structural organization [53]. Similarly, such bidentate hydrogen bonding could also be formed between guanidine groups and negatively charged carboxylates, sulfates and phosphates on cell surface. The resultant ion-pairs could then translocate across the cell membrane due to the influence of the membrane potential, which is a different pathway from conventional endocytosis [39, 54]. Although multiple mechanisms have been proposed and no universal mechanism has been agreed on, such membrane activity of guanidine groups has been reported to enable efficient cellular uptake and endosomal escape of various cargos by destabilizing the cellular as well as endosomal membranes [55]. Herein, we incorporated guanidine groups into our rational design of helical polypeptide-based non-viral vectors, and compared the gene delivery efficiencies with their amine-containing counterparts. G3 demonstrated much higher gene transfection efficiency than P3 and T3, despite their comparable DNA binding strength and cellular uptake level (**Figure 21**). Intracellular kinetics studies further suggested that G3, G6 and G8 were internalized mainly through energy-independent permeation or caveolae-mediated endocytosis, which both avoid endosomal entrapment. We speculated that such effective pathways of cell entry largely contributed to the excellent gene transfection efficiencies of the guanidine-containing polypeptides.

In addition to guanidine group, secondary structure and hydrophobicity also have impact on the membrane activities of CPPs. Therefore, we hypothesized that the inclusion of helical structures and hydrophobic content could alter the membrane activities of polypeptides and ultimately affect their gene delivery efficiencies. In comparison to PLR which adopts random coil conformation and lacks hydrophobicity, G3 possessed long hydrophobic side chains and thus was able to adopt helical conformation because the electrostatic interactions among pendant charged groups was greatly decreased. The notably enhanced pore formation properties and gene transfection efficiencies collectively substantiated the importance of the introduced helical structure and hydrophobicity. Moreover, our previous studies on the comparison of cationic polypeptides with exactly the same chemical composition yet different secondary structure (helix vs. random coil) also revealed that helical structure remarkably contributed to the strong pore formation properties of polypeptides to mediate effective gene transfection [26, 45]. Further increasing the hydrophobicity by elongating the side chain resulted in further elevated pore formation activities. As a result, G8 was able to mediate effective transfection efficiencies at the N/P ratio of 5 while comparable efficiencies were noted at the N/P ratio of 10 for G3 and G6 (**Figure 19A, 19B**). In consistence, G6 and G8 showed notably higher resistance against serum than G3, a desired property towards *in vivo* gene delivery.

The pore formation mechanism, although highly effective in triggering cellular internalization and endosomal escape, will at the same cause irreversible damage to the cell membranes at excessive levels. This holds true for guanidine-containing helical polypeptides, where longer hydrophobic side chain length rendered the polypeptides with higher membrane activities but also higher cytotoxicities. Consequently, in HeLa cells which are more vulnerable to material-induced cytotoxicity, G8 displayed decreased rather than increased gene transfection

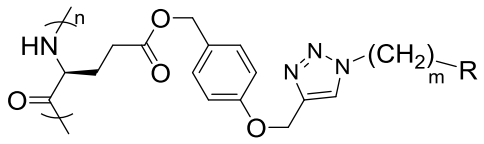
efficiency compared to G6 due to the comprised cell viability. COS-7cells were more resistant to material-induced cytotoxicity, and therefore G6 and G8 were equally efficient in COS-7 cells. Serum could shield the surface charge of the polyplexes to reduce material cytotoxicity [56], and therefore at the same DNA amount, G8 with the highest membrane activity revealed the highest transfection efficiency. At higher DNA amount (0.2 μg/well), excessive G8 displayed appreciable cytotoxicities and thus the transfection efficiency remained slightly lower than G6, the same trend as observed under serum-free condition. These results collectively suggest that an optimal balance between membrane activity and cytotoxicity is crucial towards the maximization of the gene delivery efficiencies of helical polypeptides and other polycation-based non-viral vectors.

CHAPTER 5

CONCLUSION

By taking advantage of well-controlled HMDS-mediated ROP of NCA and highly efficient "click" chemistry, a set of α-helical, cationic polypeptides with diverse charged groups as well as hydrophobic side chain lengths were synthesized and systematically investigated in terms of the effect of polypeptide structure on the gene delivery efficiencies. Incorporation of guanidine group, helical conformation and hydrophobic content into the polypeptide-based non-viral vectors collectively led to materials with high membrane activities and transfection efficiencies, outperforming LPF2000 by 2.5~5.5 folds. Although hydrophobicity enhanced the membrane activities of the polypeptides via the pore formation mechanism, excessive hydrophobicity will simultaneously cause irreversible damage to cell membranes and ultimately impair the transfection efficiencies. Therefore, a proper balance between membrane activities and cytotoxicities needs to be determined during the material design in order to maximize the efficacy of non-viral vectors. Such study on structure-function relations provides insights into the rational design of non-viral vectors and the top-performing materials identified (G6 and G8) may serve as promising additions to the existing vectors.

FIGURES AND TABLES



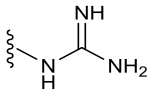
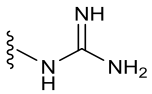
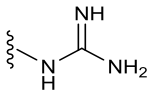
Polypeptide	m	R	Helicity (%)
G3	3		52
G6	6		59
G8	8		55
P3	3		60
T3	3		71

Table 1. Structures of amine/guanidine functionalized polypeptides.

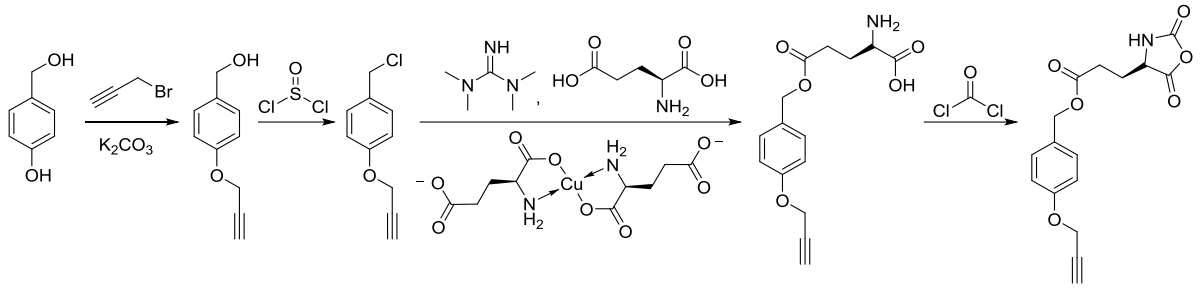


Figure 1. Synthetic routes of γ-(4-propargyloxybenzyl)-L-glutamic acid based *N*-carboxyanhydride (POB-L-Glu-NCA).

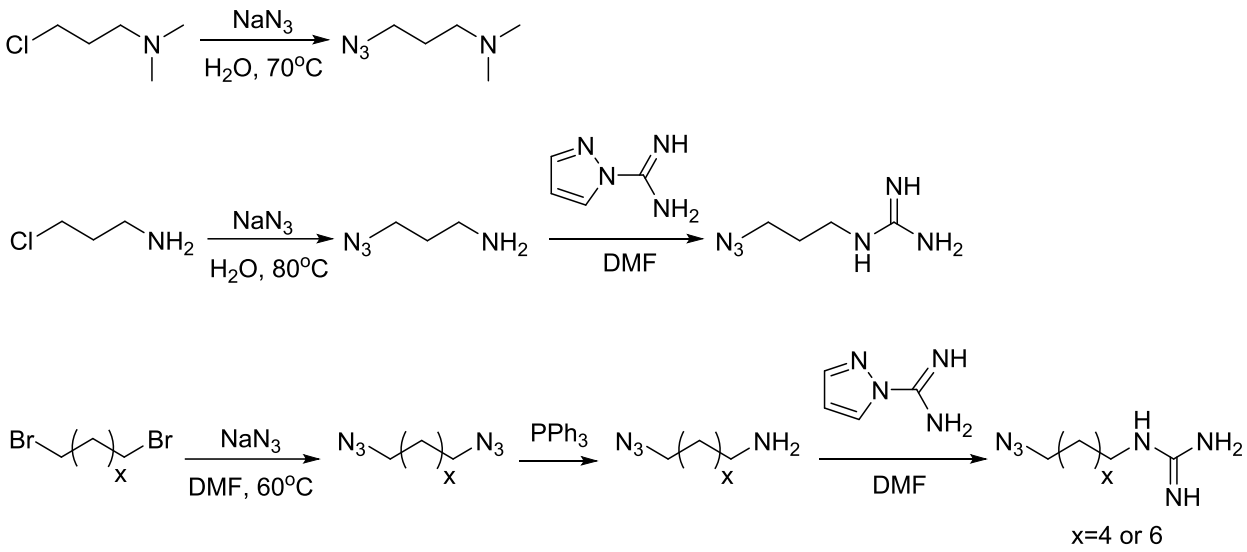


Figure 2. Synthetic routes of azido amines/guanidines.

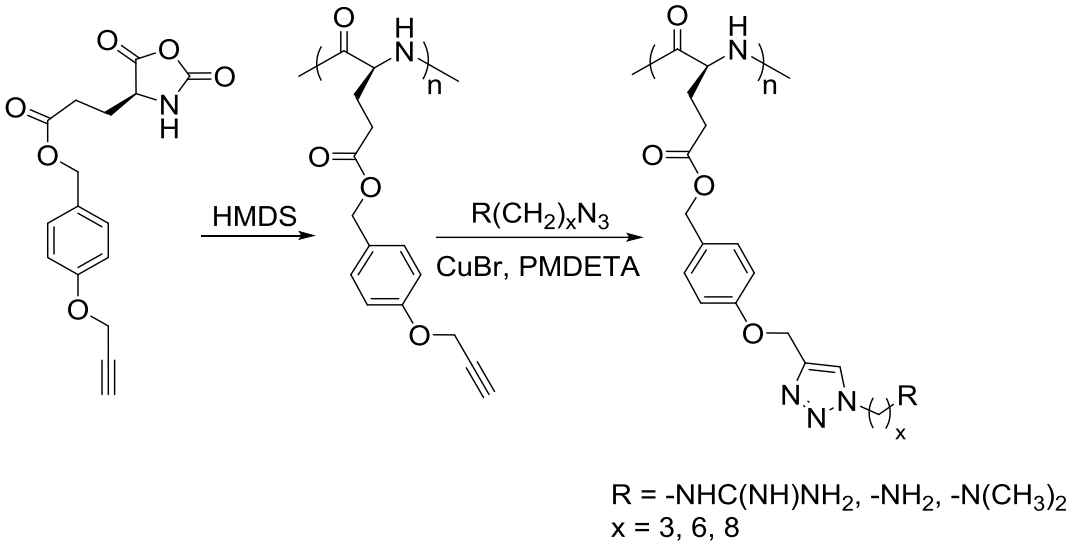


Figure 3. Synthetic route of amine/guanidine functionalized polypeptides.

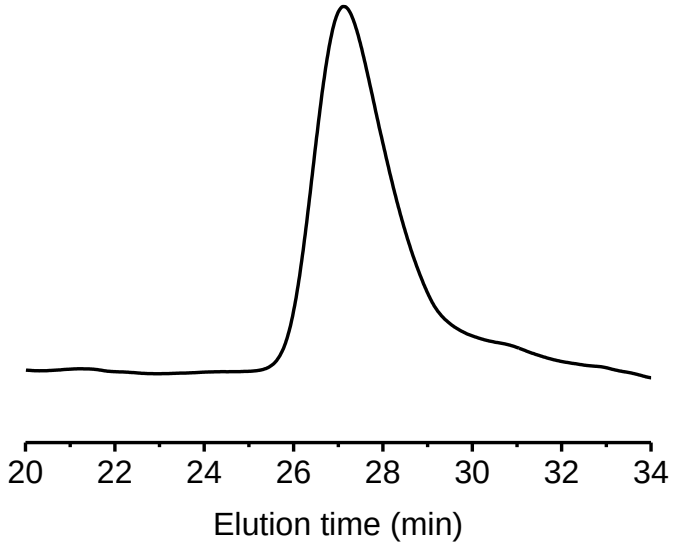


Figure 4. GPC trace of poly(γ-(4-propargyloxybenzyl)-$_{L}$-glutamate) (PPOBLG).

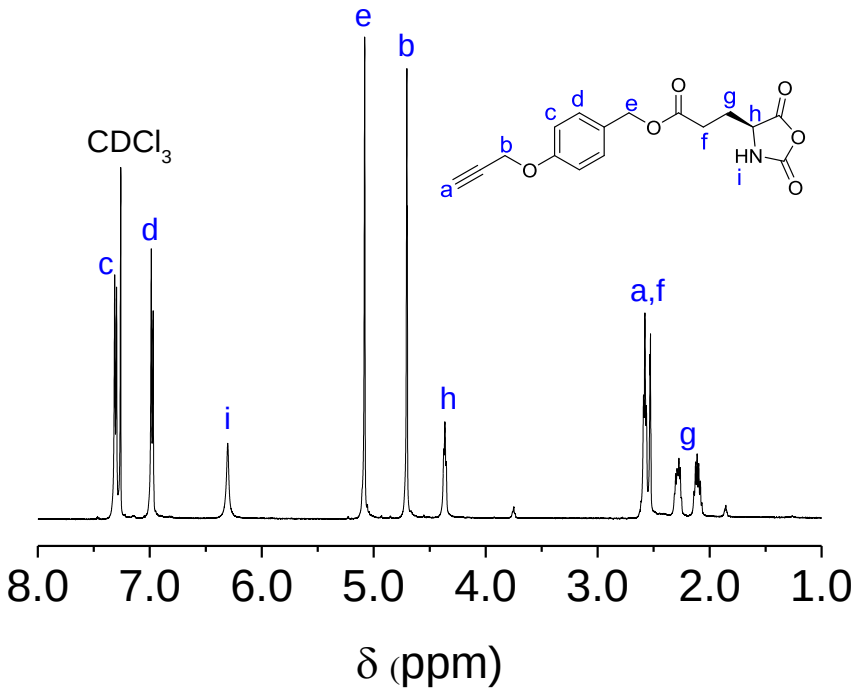


Figure 5. ^{1}H NMR spectrum of POB-L-Glu-NCA in $CDCl_3$.

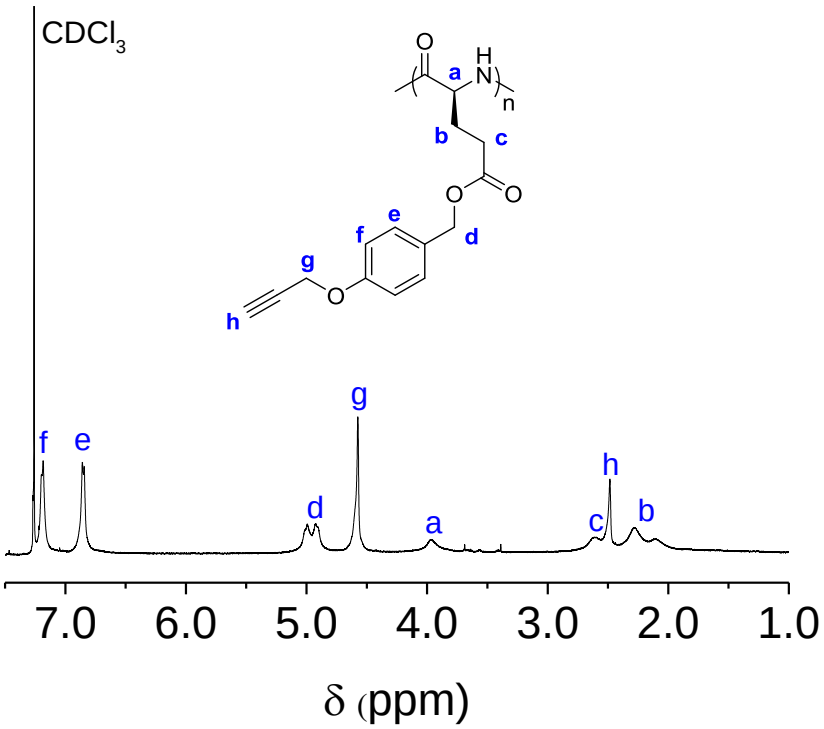


Figure 6. ^{1}H NMR spectrum of PPOBLG in $CDCl_3$.

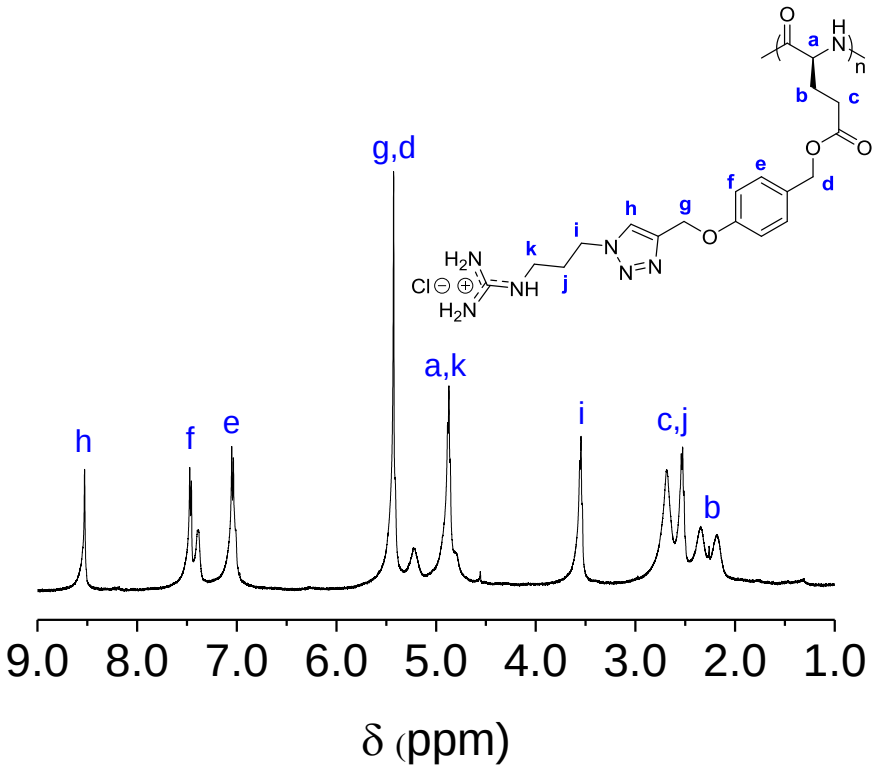


Figure 7. ^{1}H NMR spectrum of polypeptide G3 in TFA-*d*.

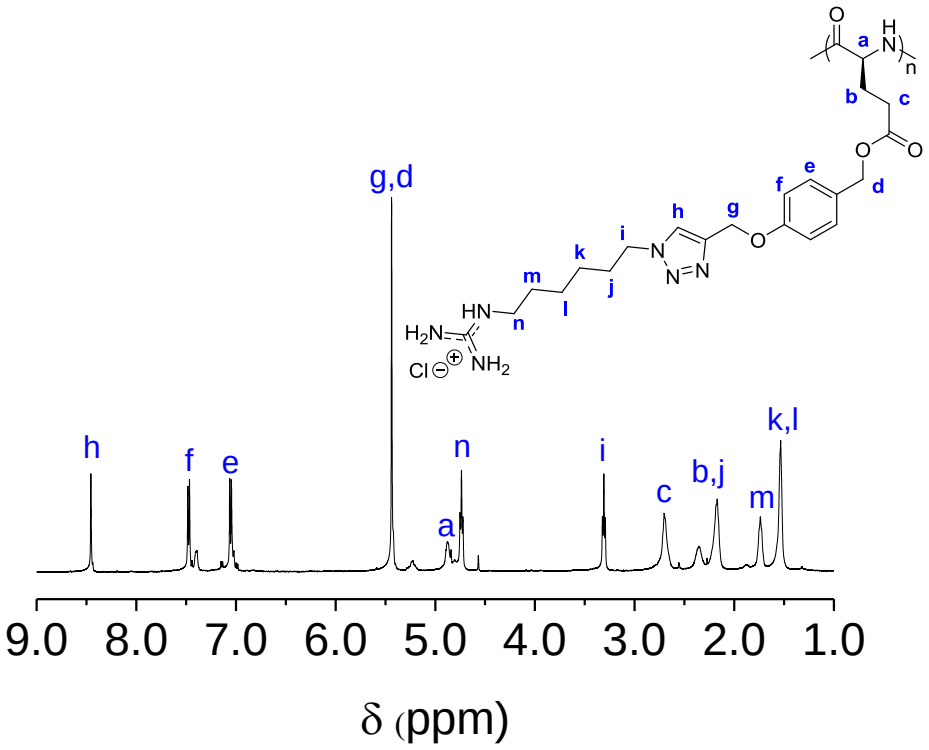


Figure 8. ^{1}H NMR spectrum of polypeptide G6 in TFA-*d*.

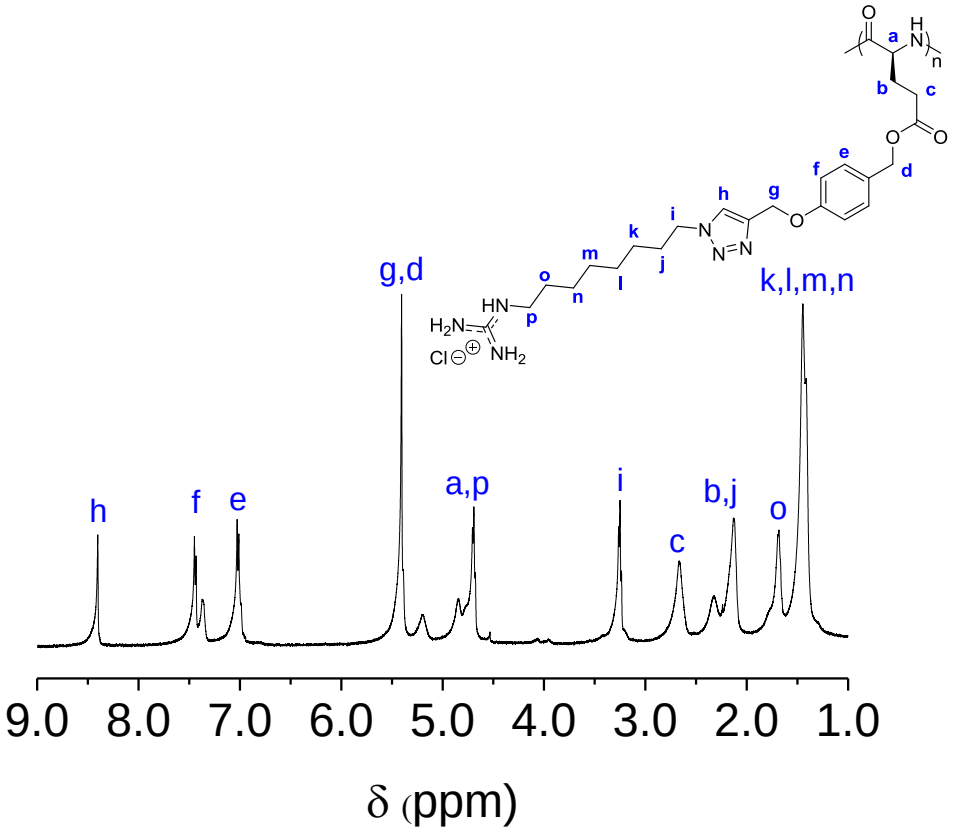


Figure 9. ^{1}H NMR spectrum of polypeptide G8 in TFA-*d*.

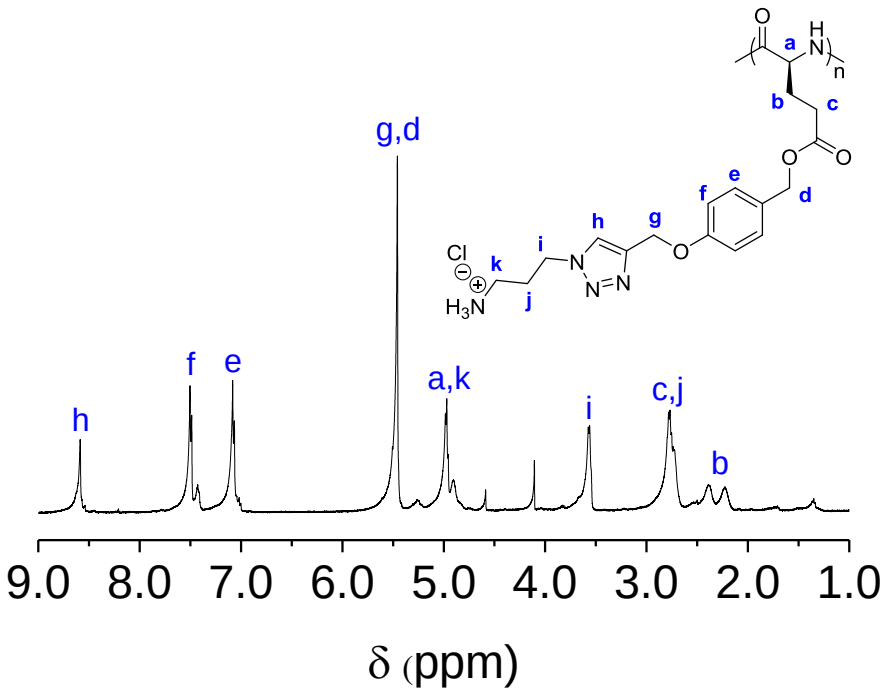


Figure 10. ^{1}H NMR spectrum of polypeptide P3 in TFA-*d*.

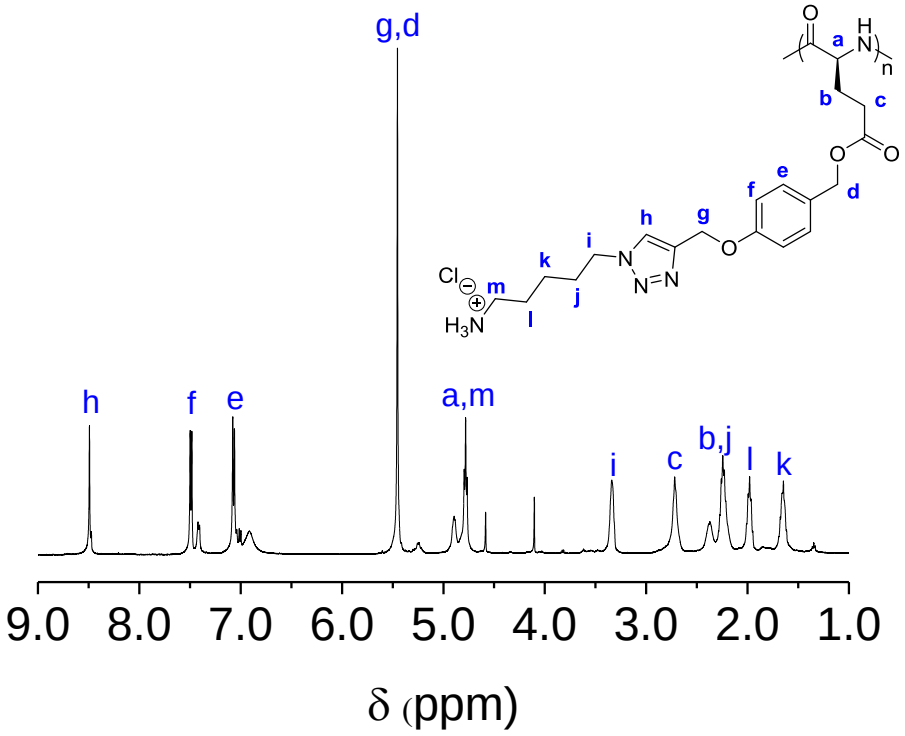


Figure 11. ^{1}H NMR spectrum of polypeptide P5 in TFA-*d*.

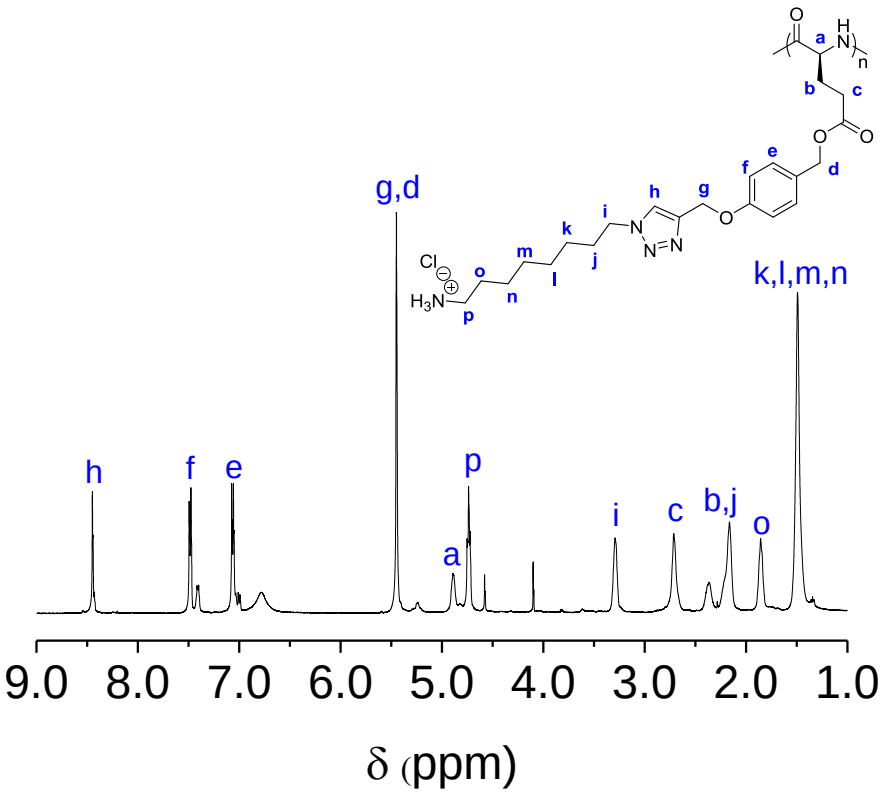


Figure 12. ^{1}H NMR spectrum of polypeptide P8 in TFA-*d*.

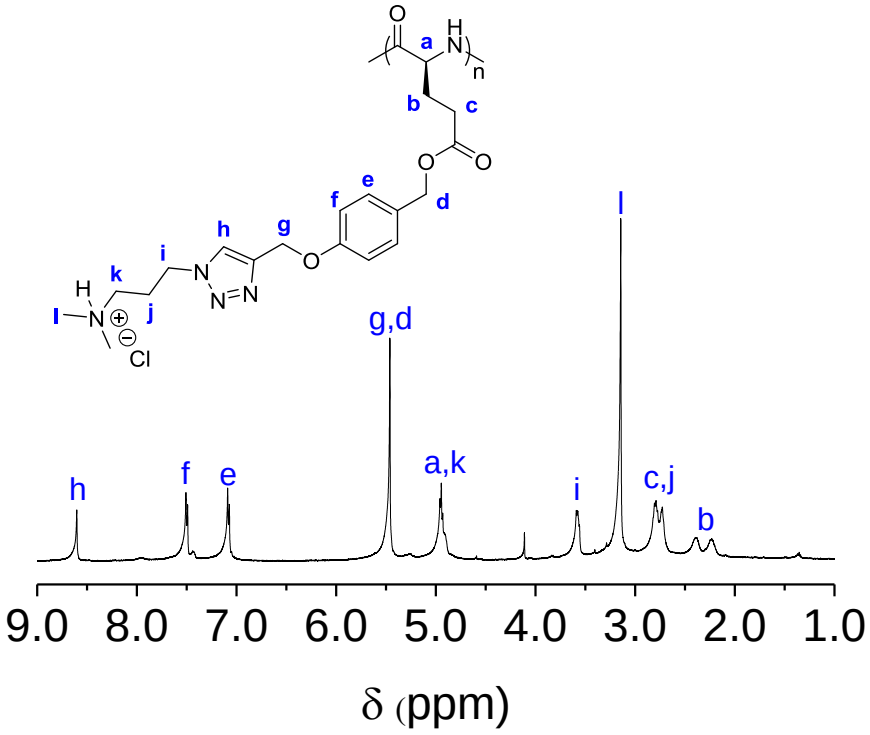


Figure 13. ^{1}H NMR spectrum of polypeptide T3 in TFA-*d*.

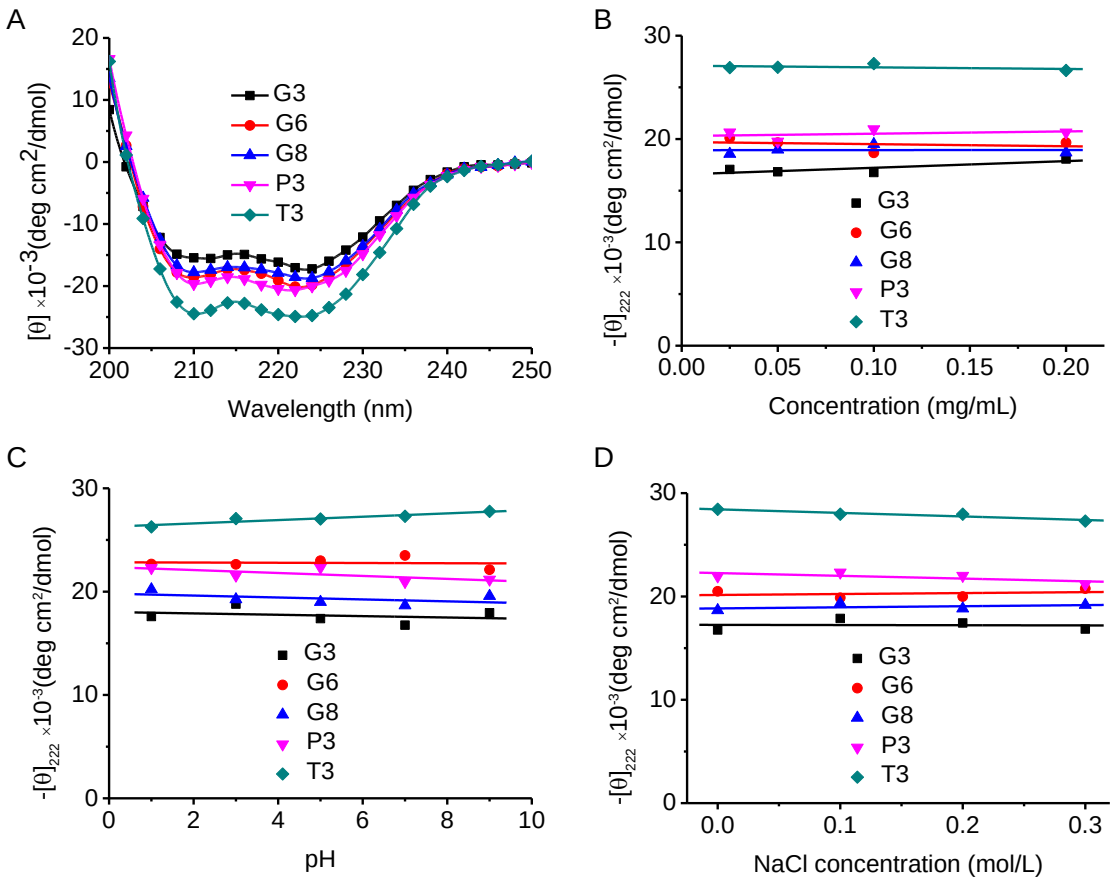


Figure 14. (A) CD spectra of polypeptides (0.1 mg/mL) in the aqueous solution (pH 7.0). Helical stability against polypeptide concentration (B), pH (C) and NaCl concentration (D) as indicated by the molar ellipticity at 222 nm.

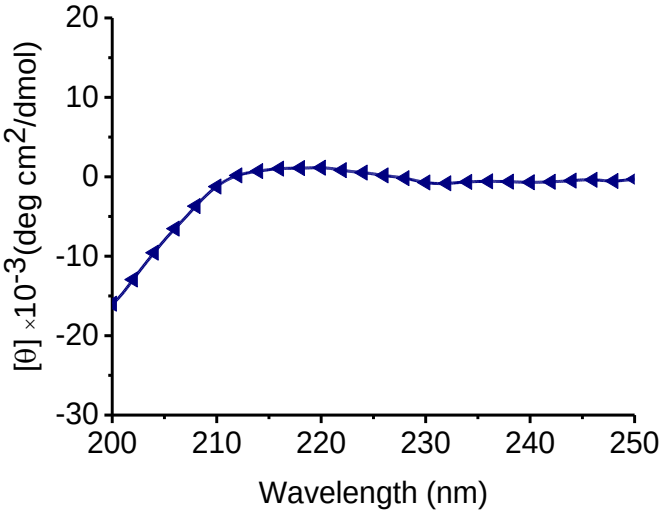


Figure 15. CD spectrum of PLR in water (0.1 mg/mL) at pH 7.

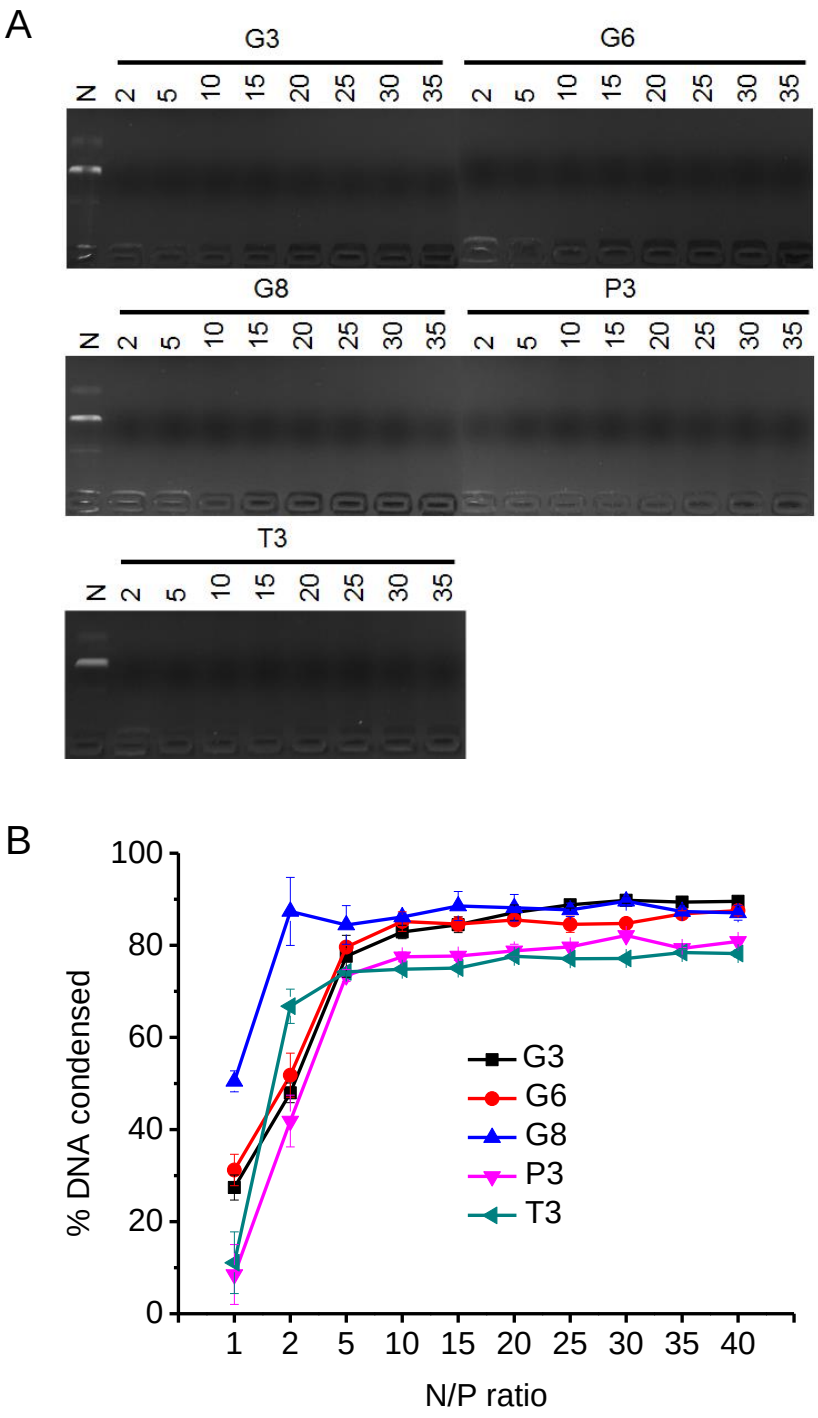


Figure 16. DNA condensation by polypeptides at various N/P ratios as evaluated by the gel retardation assay (A) and EB exclusion assay (B). N represents naked DNA.

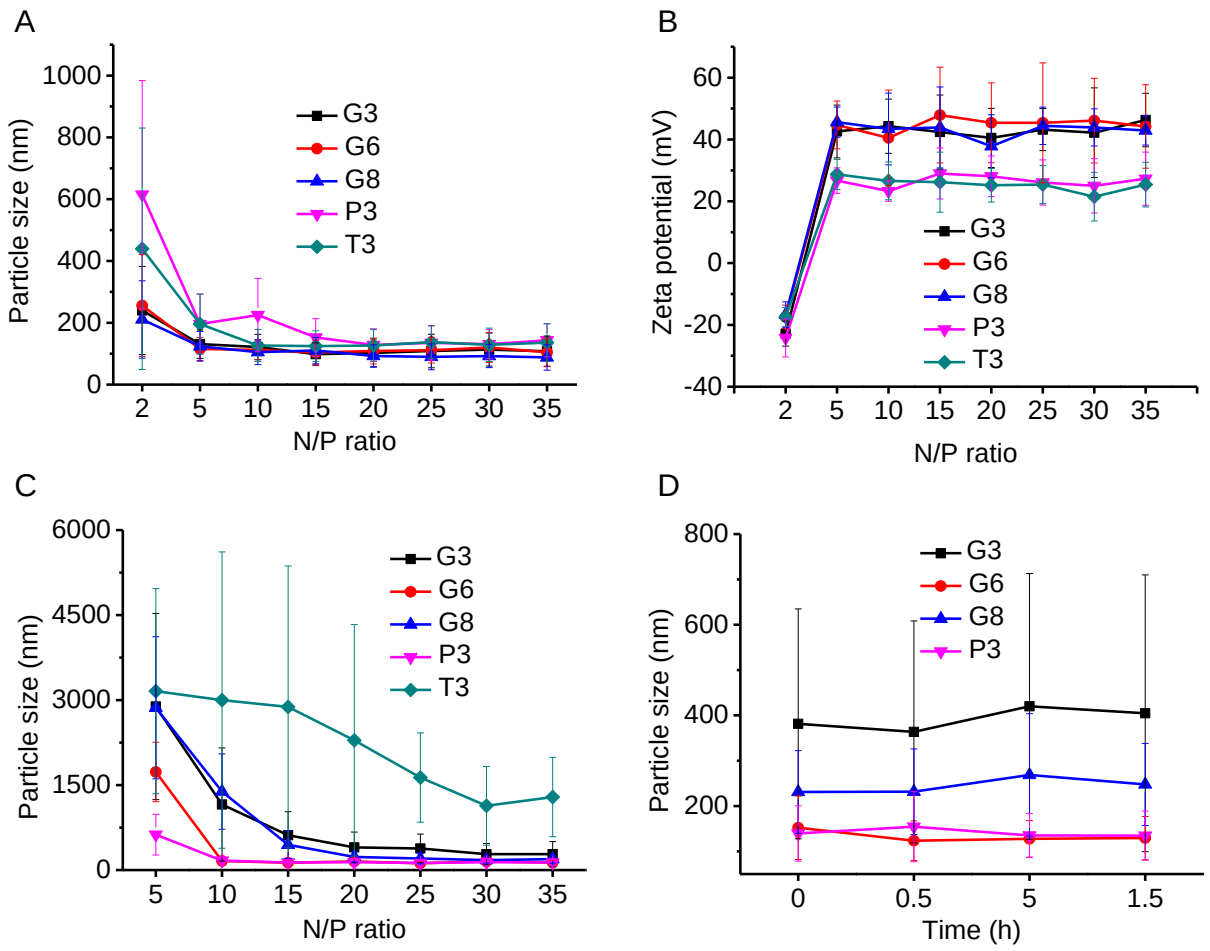


Figure 17. Particle size (A) and zeta potential (B) of polyplexes in DI water at various N/P ratios as determined by DLS measurement. (C) Particle size of polyplexes at various N/P ratios prepared in PBS. (D) Alteration of particle size of polyplexes (N/P = 20, prepared in PBS) upon dilution with PBS (x 50 fold).

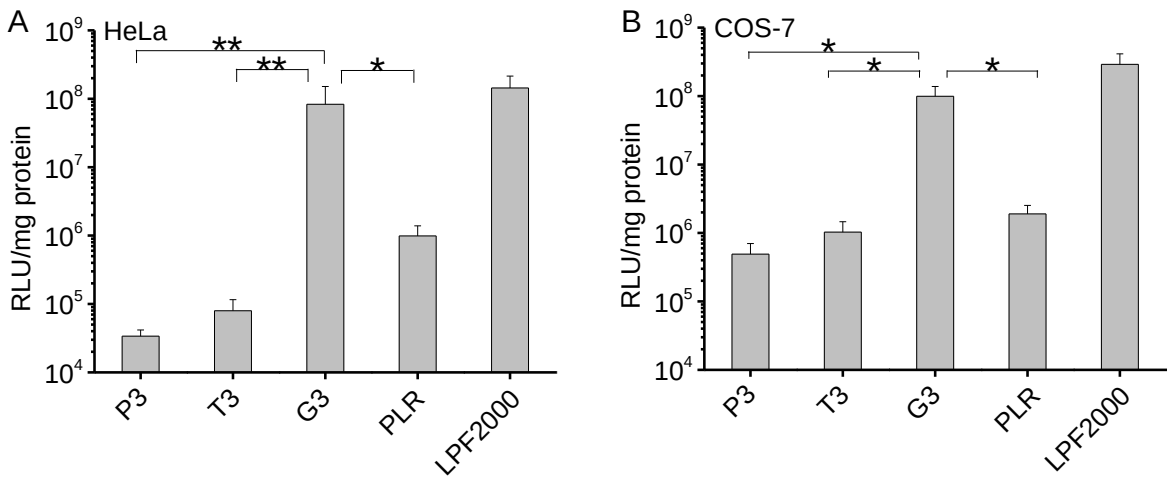


Figure 18. *In vitro* transfection efficiencies of polyplexes (N/P = 10) in HeLa (A) and COS-7 (B) cells. PLR and LPF2000 were included as positive controls.

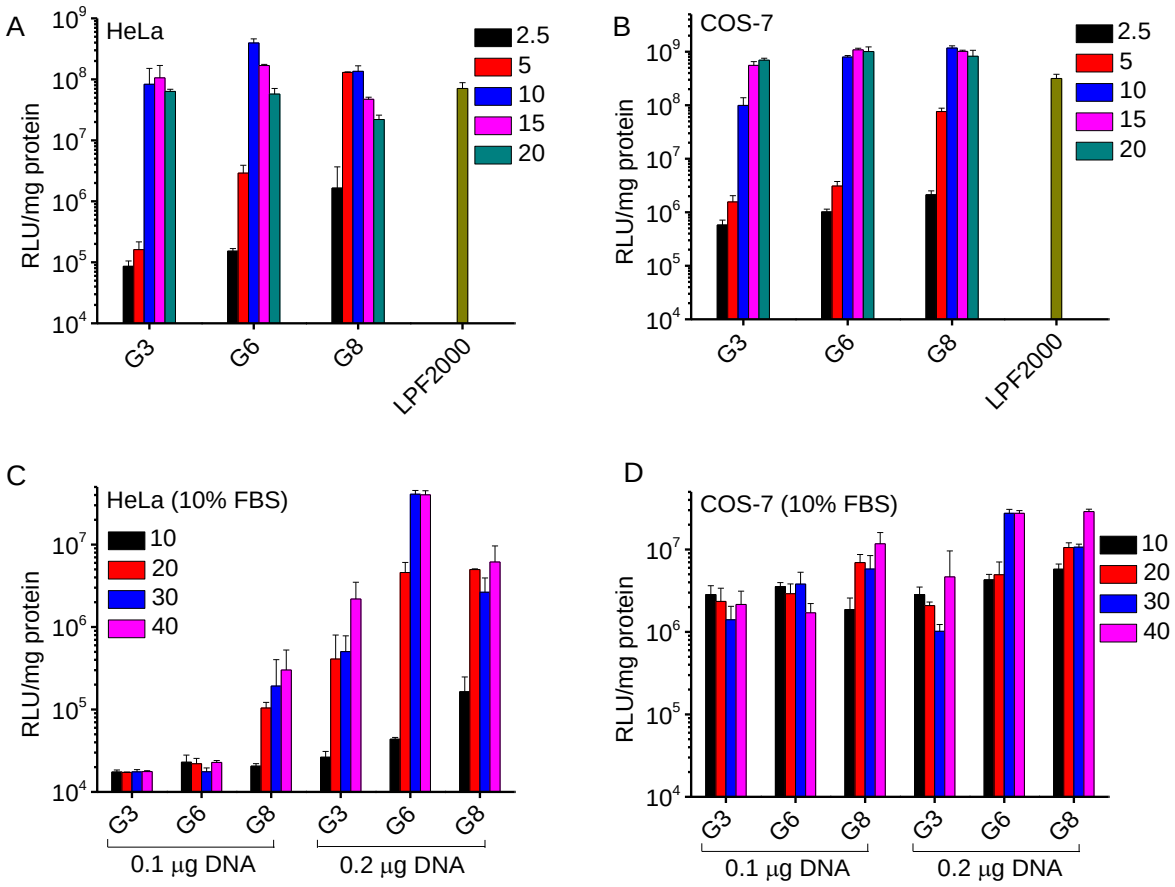


Figure 19. *In vitro* transfection efficiencies of polyplexes at various N/P ratios in HeLa (A) and COS-7 (B) cells in the serum-free medium. Transfection efficiencies in HeLa (C) and COS-7 (D) cells in the presence of serum.

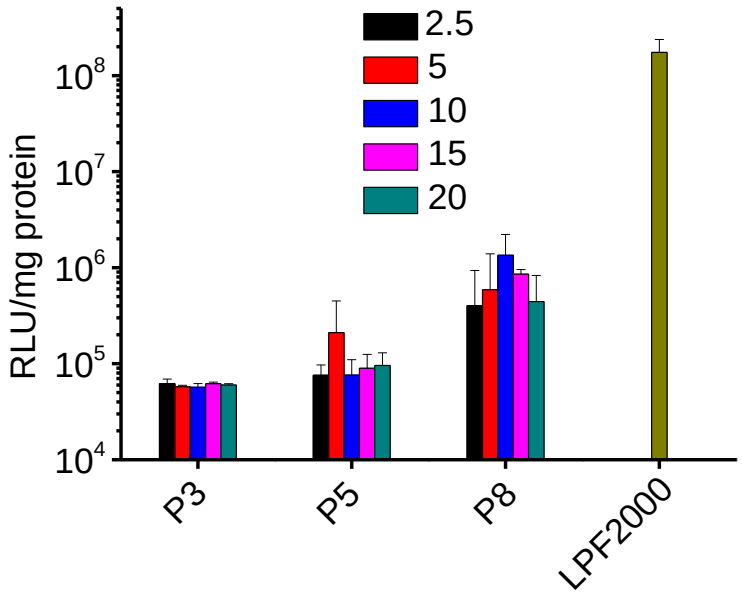


Figure 20. *In vitro* transfection efficiencies of polyplexes at various N/P ratios in HeLa cells.

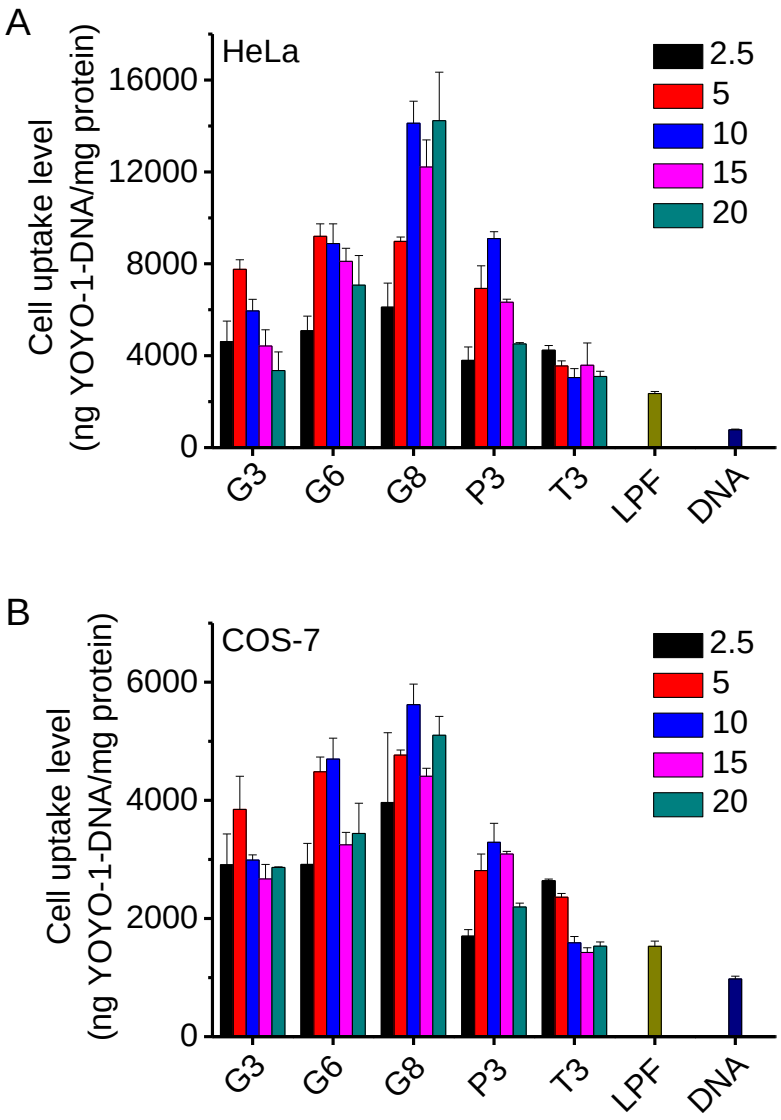


Figure 21. Cellular uptake levels of polypeptide/YOYO-1-DNA polyplexes in HeLa (A) and COS-7 (B) cells at various N/P ratios.

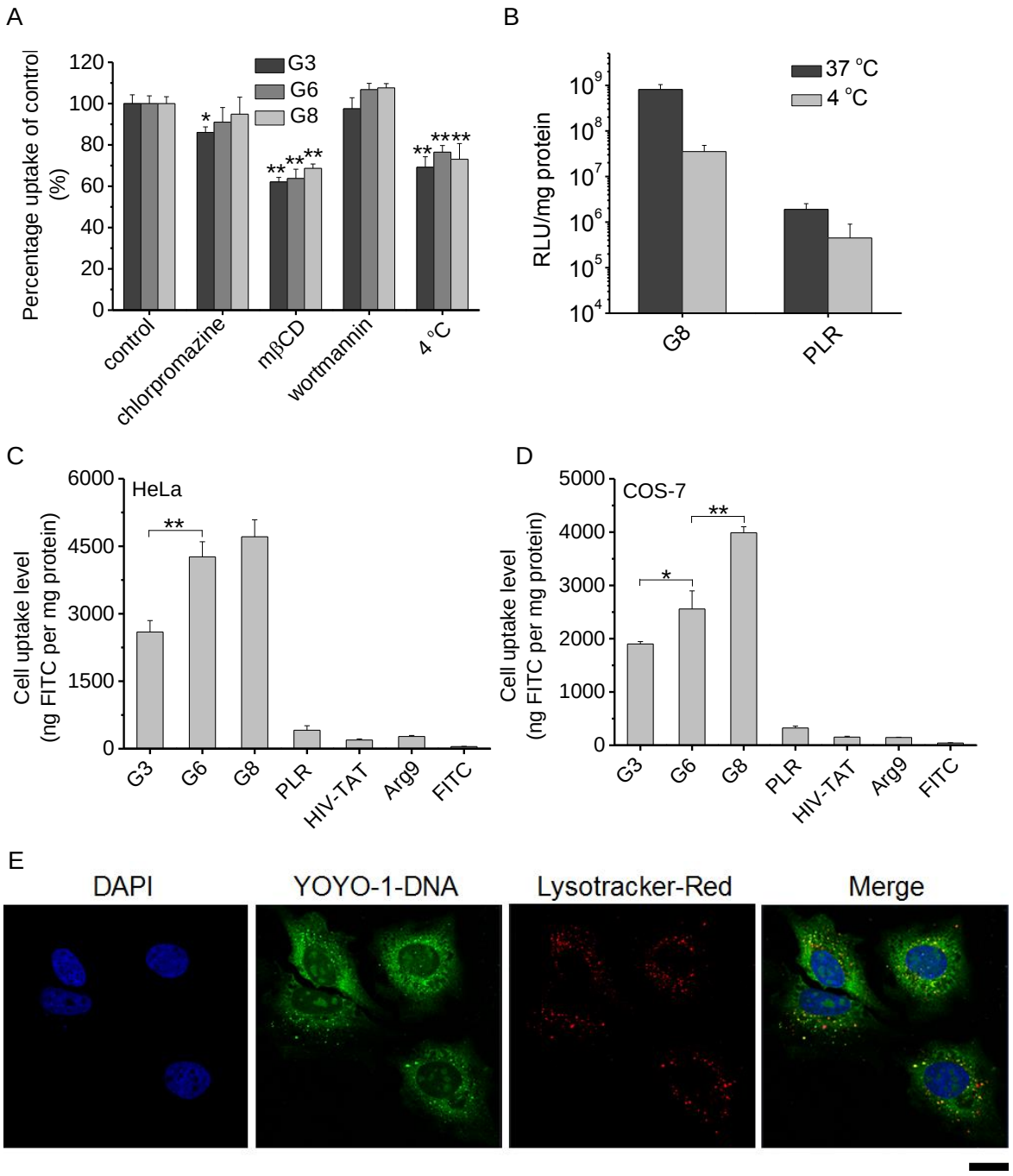


Figure 22. Intracellular kinetics of polypeptide/YOYO-1-DNA polyplexes. (A) Cellular uptake of polyplexes (N/P = 10) in COS-7 cells at 4 ℃ or in the presence of various endocytic inhibitors. (B) Transfection efficiencies of polyplexes (N/P = 10) at 4 ℃ and 37 ℃ in COS-7 cells. (C) Cell uptake level of FITC-Tris in HeLa (C) and COS-7 (D) cells following co-incubation with the polypeptides for 2 h at 37 ℃. (E) CLSM images of HeLa cells following incubation with G6/YOYO-1-DNA polyplexes (N/P = 10) at 37 ℃ for 4 h. Bar represented 20 μm.

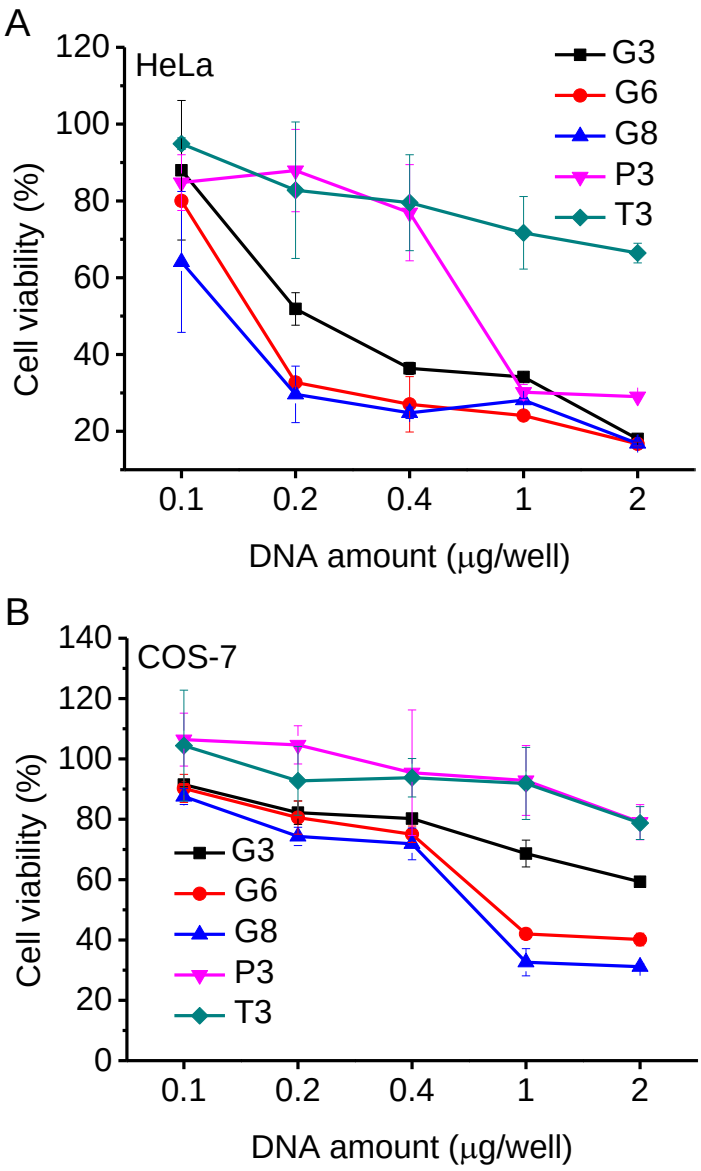


Figure 23. Cytotoxicity of polyplexes (N/P = 10) towards HeLa (A) and COS-7 (B) cells as determined by the MTT assay.

REFERENCES

[1] Candolfi M, Xiong W, Yagiz K, Liu C, Muhammad AK, Puntel M, et al. Gene therapy-mediated delivery of targeted cytotoxins for glioma therapeutics. Proc Natl Acad Sci U S A. 2010;107:20021-6.

[2] Fellowes R, Etheridge CJ, Coade S, Cooper RG, Stewart L, Miller AD, et al. Amelioration of established collagen induced arthritis by systemic IL-10 gene delivery. Gene Ther. 2000;7:967-77.

[3] Lotze MT, Kost TA. Viruses as gene delivery vectors: Application to gene function, target validation, and assay development. Cancer Gene Ther. 2002;9:692-9.

[4] Daya S, Berns KI. Gene Therapy Using Adeno-Associated Virus Vectors. Clin Microbiol Rev. 2008;21:583-93.

[5] Kay MA, Glorioso JC, Naldini L. Viral vectors for gene therapy: the art of turning infectious agents into vehicles of therapeutics. Nat Med. 2001;7:33-40.

[6] Thomas CE, Ehrhardt A, Kay MA. Progress and problems with the use of viral vectors for gene therapy. Nat Rev Genet. 2003;4:346-58.

[7] Yamanouchi D, Wu J, Lazar AN, Kent KC, Chu CC, Liu B. Biodegradable arginine-based poly(ester-amide)s as non-viral gene delivery reagents. Biomaterials. 2008;29:3269-77.

[8] Masuda T, Akita H, Nishio T, Niikura K, Kogure K, Ijiro K, et al. Development of lipid particles targeted via sugar-lipid conjugates as novel nuclear gene delivery system. Biomaterials. 2008;29:709-23.

[9] Zhang QF, Yi WJ, Wang B, Zhang J, Ren LF, Chen QM, et al. Linear polycations by ring-opening polymerization as non-viral gene delivery vectors. Biomaterials. 2013;34:5391-401.

[10] Derossi D, Calvet S, Trembleau A, Brunissen A, Chassaing G, Prochiantz A. Cell internalization of the third helix of the antennapedia homeodomain is receptor-independent. Journal of Biological Chemistry. 1996;271:18188-93.

[11] Heitz F, Morris MC, Divita G. Twenty years of cell-penetrating peptides: from molecular mechanisms to therapeutics. Brit J Pharmacol. 2009;157:195-206.

[12] Dobson CM. Protein folding and misfolding. Nature. 2003;426:884-90.

[13] Munoz V, Serrano L. Elucidating the Folding Problem of Helical Peptides Using Empirical Parameters. Nat Struct Biol. 1994;1:399-409.

[14] Daniels DS, Schepartz A. Intrinsically cell-permeable miniature proteins based on a minimal cationic PPII motif. J Am Chem Soc. 2007;129:14578-+.

[15] Kolusheva S, Shahal T, Jelinek R. Peptide-membrane interactions studied by a new phospholipid/polydiacetylene colorimetric vesicle assay. Biochemistry-Us. 2000;39:15851-9.

[16] Brooks H, Lebleu B, Vives E. Tat peptide-mediated cellular delivery: back to basics. Adv Drug Deliver Rev. 2005;57:559-77.

[17] Terrone D, Sang SLW, Roudaia L, Silvius JR. Penetratin and related cell-penetrating cationic peptides can translocate across lipid bilayers in the presence of a transbilayer potential. Biochemistry-Us. 2003;42:13787-99.

[18] Pooga M, Hallbrink M, Zorko M, Langel U. Cell penetration by transportan. Faseb J. 1998;12:67-77.

[19] Martin ME, Rice KG. Peptide-guided gene delivery. Aaps Journal. 2007;9:E18-E29.

[20] Zhang X, Oulad-Abdelghani M, Zelkin AN, Wang YJ, Haikel Y, Mainard D, et al. Poly(L-lysine) nanostructured particles for gene delivery and hormone stimulation. Biomaterials. 2010;31:1699-706.

[21] Choi YH, Liu F, Kim JS, Choi YK, Park JS, Kim SW. Polyethylene glycol-grafted poly-L-lysine as polymeric gene carrier. J Control Release. 1998;54:39-48.

[22] Lee H, Jeong JH, Park TG. PEG grafted polylysine with fusogenic peptide for gene delivery: high transfection efficiency with low cytotoxicity. J Control Release. 2002;79:283-91.

[23] Okuda T, Sugiyama A, Niidome T, Aoyagi H. Characters of dendritic poly((L)-lysine) analogues with the terminal lysines replaced with arginines and histidines as gene carriers in vitro. Biomaterials. 2004;25:537-44.

[24] Lu H, Wang J, Bai YG, Lang JW, Liu SY, Lin Y, et al. Ionic polypeptides with unusual helical stability. Nat Commun. 2011;2.

[25] Gabrielson NP, Lu H, Yin LC, Li D, Wang F, Cheng JJ. Reactive and Bioactive Cationic a-Helical Polypeptide Template for Nonviral Gene Delivery. Angew Chem Int Edit. 2012;51:1143-7.

[26] Gabrielson NP, Lu H, Yin LC, Kim KH, Cheng JJ. A Cell-penetrating Helical Polymer For siRNA Delivery to Mammalian Cells. Mol Ther. 2012;20:1599-609.

[27] Yin LC, Song ZY, Kim KH, Zheng N, Tang HY, Lu H, et al. Reconfiguring the architectures of cationic helical polypeptides to control non-viral gene delivery. Biomaterials. 2013;34:2340-9.
[28] Bishop CJ, Ketola TM, Tzeng SY, Sunshine JC, Urtti A, Lemmetyinen H, et al. The effect and role of carbon atoms in poly(beta-amino ester)s for DNA binding and gene delivery. J Am Chem Soc. 2013;135:6951-7.
[29] Fang C, Kievit FM, Cho YC, Mok H, Press OW, Zhang M. Effect of cationic side-chains on intracellular delivery and cytotoxicity of pH sensitive polymer-doxorubicin nanocarriers. Nanoscale. 2012;4:7012-20.
[30] Wender PA, Galliher WC, Goun EA, Jones LR, Pillow TH. The design of guanidinium-rich transporters and their internalization mechanisms. Adv Drug Deliver Rev. 2008;60:452-72.
[31] Som A, Reuter A, Tew GN. Protein transduction domain mimics: the role of aromatic functionality. Angewandte Chemie. 2012;51:980-3.
[32] Som A, Tezgel AO, Gabriel GJ, Tew GN. Self-activation in de novo designed mimics of cell-penetrating peptides. Angewandte Chemie. 2011;50:6147-50.
[33] Lu H, Cheng J. Hexamethyldisilazane-mediated controlled polymerization of alpha-amino acid N-carboxyanhydrides. J Am Chem Soc. 2007;129:14114-5.
[34] Morrow JA, Segall ML, Lund-Katz S, Phillips MC, Knapp M, Rupp B, et al. Differences in stability among the human apolipoprotein E isoforms determined by the amino-terminal domain. Biochemistry-Us. 2000;39:11657-66.
[35] Zhao X, Yin LC, Ding JY, Tang C, Gu SH, Yin CH, et al. Thiolated trimethyl chitosan nanocomplexes as gene carriers with high in vitro and in vivo transfection efficiency. J Control Release. 2010;144:46-54.
[36] Ter-Avetisyan G, Tuennemann G, Nowak D, Nitschke M, Herrmann A, Drab M, et al. Cell Entry of Arginine-rich Peptides Is Independent of Endocytosis. Journal of Biological Chemistry. 2009;284:3370-8.
[37] Yin L, Song Z, Kim KH, Zheng N, Tang H, Lu H, et al. Reconfiguring the architectures of cationic helical polypeptides to control non-viral gene delivery. Biomaterials. 2013;34:2340-9.
[38] Engler AC, Lee HI, Hammond PT. Highly Efficient "Grafting onto" a Polypeptide Backbone Using Click Chemistry. Angew Chem Int Edit. 2009;48:9334-8.

[39] Rothbard JB, Jessop TC, Wender PA. Adaptive translocation: the role of hydrogen bonding and membrane potential in the uptake of guanidinium-rich transporters into cells. Adv Drug Deliver Rev. 2005;57:495-504.
[40] Nchinda G, Uberla K, Zschornig O. Characterization of cationic lipid/DNA transfection complexes differing in susceptability to inhibition by serum. J Liposome Res. 2003;13:95-.
[41] Khalil IA, Kogure K, Akita H, Harashima H. Uptake pathways and subsequent intracellular trafficking in nonviral gene delivery. Pharmacological reviews. 2006;58:32-45.
[42] Pantos A, Tsogas I, Paleos CA. Guanidinium group: A versatile moiety inducing transport and multicompartmentalization in complementary membranes. Bba-Biomembranes. 2008;1778:811-23.
[43] Gratton SE, Ropp PA, Pohlhaus PD, Luft JC, Madden VJ, Napier ME, et al. The effect of particle design on cellular internalization pathways. Proc Natl Acad Sci U S A. 2008;105:11613-8.
[44] Pack DW, Hoffman AS, Pun S, Stayton PS. Design and development of polymers for gene delivery. Nat Rev Drug Discov. 2005;4:581-93.
[45] Yin L, Song Z, Kim KH, Zheng N, Gabrielson NP, Cheng J. Non-Viral Gene Delivery via Membrane-Penetrating, Mannose-Targeting Supramolecular Self-Assembled Nanocomplexes (Adv. Mater. 22/2013). Adv Mater. 2013;25:3062-.
[46] Tang H, Yin L, Kim KH, Cheng J. Helical poly(arginine) mimics with superior cell-penetrating and molecular transporting properties. Chemical Science. 2013;4:3839-44.
[47] Tian HY, Deng C, Lin H, Sun J, Deng M, Chen X, et al. Biodegradable cationic PEG-PEI-PBLG hyperbranched block copolymer: synthesis and micelle characterization. Biomaterials. 2005;26:4209-17.
[48] Godbey WT, Wu KK, Mikos AG. Tracking the intracellular path of poly(ethylenimine)/DNA complexes for gene delivery. Proc Natl Acad Sci U S A. 1999;96:5177-81.
[49] Rejman J, Bragonzi A, Conese M. Role of clathrin- and caveolae-mediated endocytosis in gene transfer mediated by lipo- and polyplexes. Mol Ther. 2005;12:468-74.
[50] Behr JP. The proton sponge: A trick to enter cells the viruses did not exploit. Chimia. 1997;51:34-6.

[51] Funhoff AM, van Nostrum CF, Koning GA, Schuurmans-Nieuwenbroek NME, Crommelin DJA, Hennink WE. Endosomal escape of polymeric gene delivery complexes is not always enhanced by polymers buffering at low pH. Biomacromolecules. 2004;5:32-9.

[52] Benjaminsen RV, Mattebjerg MA, Henriksen JR, Moghimi SM, Andresen TL. The Possible "Proton Sponge" Effect of Polyethylenimine (PEI) Does Not Include Change in Lysosomal pH. Mol Ther. 2013;21:149-57.

[53] Aissaoui A, Oudrhiri N, Petit L, Hauchecorne M, Kan E, Sainlos M, et al. Progress in gene delivery by cationic lipids: Guanidinium-cholesterol-based systems as an example. Curr Drug Targets. 2002;3:1-16.

[54] Rothbard JB, Jessop TC, Lewis RS, Murray BA, Wender PA. Role of membrane potential and hydrogen bonding in the mechanism of translocation of guanidinium-rich peptides into cells. J Am Chem Soc. 2004;126:9506-7.

[55] Stanzl EG, Trantow BM, Vargas JR, Wender PA. Fifteen Years of Cell-Penetrating, Guanidinium-Rich Molecular Transporters: Basic Science, Research Tools, and Clinical Applications. Accounts of chemical research. 2013.

[56] Audouy S, Molema G, de Leij L, Hoekstra D. Serum as a modulator of lipoplex-mediated gene transfection: dependence of amphiphile, cell type and complex stability. J Gene Med. 2000;2:465-76.